Measurement of the forward-backward asymmetry in the distribution of leptons in tt[over ¯] events in the lepton+jets channel

V. M. Abazov *et al.* (D0 Collaboration)

Measurement of the forward-backward asymmetry in the distribution of leptons in $t\bar{t}$ events in the lepton+jets channel

V.M. Abazov,[31] B. Abbott,[67] B.S. Acharya,[25] M. Adams,[46] T. Adams,[44] J.P. Agnew,[41] G.D. Alexeev,[31]
G. Alkhazov,[35] A. Alton[a],[56] A. Askew,[44] S. Atkins,[54] K. Augsten,[7] C. Avila,[5] F. Badaud,[10] L. Bagby,[45]
B. Baldin,[45] D.V. Bandurin,[73] S. Banerjee,[25] E. Barberis,[55] P. Baringer,[53] J.F. Bartlett,[45] U. Bassler,[15]
V. Bazterra,[46] A. Bean,[53] M. Begalli,[2] L. Bellantoni,[45] S.B. Beri,[23] G. Bernardi,[14] R. Bernhard,[19] I. Bertram,[39]
M. Besançon,[15] R. Beuselinck,[40] P.C. Bhat,[45] S. Bhatia,[58] V. Bhatnagar,[23] G. Blazey,[47] S. Blessing,[44] K. Bloom,[59]
A. Boehnlein,[45] D. Boline,[64] E.E. Boos,[33] G. Borissov,[39] M. Borysova[l],[38] A. Brandt,[70] O. Brandt,[20] R. Brock,[57]
A. Bross,[45] D. Brown,[14] X.B. Bu,[45] M. Buehler,[45] V. Buescher,[21] V. Bunichev,[33] S. Burdin[b],[39] C.P. Buszello,[37]
E. Camacho-Pérez,[28] B.C.K. Casey,[45] H. Castilla-Valdez,[28] S. Caughron,[57] S. Chakrabarti,[64] K.M. Chan,[51]
A. Chandra,[72] A. Chapelain,[15] E. Chapon,[15] G. Chen,[53] S.W. Cho,[27] S. Choi,[27] B. Choudhary,[24] S. Cihangir,[45]
D. Claes,[59] J. Clutter,[53] M. Cooke[k],[45] W.E. Cooper,[45] M. Corcoran,[72] F. Couderc,[15] M.-C. Cousinou,[12]
D. Cutts,[69] A. Das,[42] G. Davies,[40] S.J. de Jong,[29, 30] E. De La Cruz-Burelo,[28] F. Déliot,[15] R. Demina,[63]
D. Denisov,[45] S.P. Denisov,[34] S. Desai,[45] C. Deterre[c],[20] K. DeVaughan,[59] H.T. Diehl,[45] M. Diesburg,[45] P.F. Ding,[41]
A. Dominguez,[59] A. Dubey,[24] L.V. Dudko,[33] A. Duperrin,[12] S. Dutt,[23] M. Eads,[47] D. Edmunds,[57]
J. Ellison,[43] V.D. Elvira,[45] Y. Enari,[14] H. Evans,[49] V.N. Evdokimov,[34] A. Falkowski[m],[15] L. Feng,[47]
T. Ferbel,[63] F. Fiedler,[21] F. Filthaut,[29, 30] W. Fisher,[57] H.E. Fisk,[45] M. Fortner,[47] H. Fox,[39] S. Fuess,[45]
P.H. Garbincius,[45] A. Garcia-Bellido,[63] J.A. García-González,[28] V. Gavrilov,[32] W. Geng,[12, 57] C.E. Gerber,[46]
Y. Gershtein,[60] G. Ginther,[45, 63] G. Golovanov,[31] P.D. Grannis,[64] S. Greder,[16] H. Greenlee,[45] G. Grenier,[17]
Ph. Gris,[10] J.-F. Grivaz,[13] A. Grohsjean[c],[15] S. Grünendahl,[45] M.W. Grünewald,[26] T. Guillemin,[13] G. Gutierrez,[45]
P. Gutierrez,[67] J. Haley,[68] L. Han,[4] K. Harder,[41] A. Harel,[63] J.M. Hauptman,[52] J. Hays,[40] T. Head,[41]
T. Hebbeker,[18] D. Hedin,[47] H. Hegab,[68] A.P. Heinson,[43] U. Heintz,[69] C. Hensel,[1] I. Heredia-De La Cruz[d],[28]
K. Herner,[45] G. Hesketh[f],[41] M.D. Hildreth,[51] R. Hirosky,[73] T. Hoang,[44] J.D. Hobbs,[64] B. Hoeneisen,[9] J. Hogan,[72]
M. Hohlfeld,[21] J.L. Holzbauer,[58] I. Howley,[70] Z. Hubacek,[7, 15] V. Hynek,[7] I. Iashvili,[62] Y. Ilchenko,[71]
R. Illingworth,[45] A.S. Ito,[45] S. Jabeen,[69] M. Jaffré,[13] A. Jayasinghe,[67] M.S. Jeong,[27] R. Jesik,[40] P. Jiang,[4]
K. Johns,[42] E. Johnson,[57] M. Johnson,[45] A. Jonckheere,[45] P. Jonsson,[40] J. Joshi,[43] A.W. Jung,[45] A. Juste,[36]
E. Kajfasz,[12] D. Karmanov,[33] I. Katsanos,[59] R. Kehoe,[71] S. Kermiche,[12] N. Khalatyan,[45] A. Khanov,[68]
A. Kharchilava,[62] Y.N. Kharzheev,[31] I. Kiselevich,[32] J.M. Kohli,[23] A.V. Kozelov,[34] J. Kraus,[58] A. Kumar,[62]
A. Kupco,[8] T. Kurča,[17] V.A. Kuzmin,[33] S. Lammers,[49] P. Lebrun,[17] H.S. Lee,[27] S.W. Lee,[52] W.M. Lee,[45] X. Lei,[42]
J. Lellouch,[14] D. Li,[14] H. Li,[73] L. Li,[43] Q.Z. Li,[45] J.K. Lim,[27] D. Lincoln,[45] J. Linnemann,[57] V.V. Lipaev,[34]
R. Lipton,[45] H. Liu,[71] Y. Liu,[4] A. Lobodenko,[35] M. Lokajicek,[8] R. Lopes de Sa,[64] R. Luna-Garcia[g],[28]
A.L. Lyon,[45] A.K.A. Maciel,[1] R. Madar,[19] R. Magaña-Villalba,[28] S. Malik,[59] V.L. Malyshev,[31] J. Mansour,[20]
J. Martínez-Ortega,[28] R. McCarthy,[64] C.L. McGivern,[41] M.M. Meijer,[29, 30] A. Melnitchouk,[45] D. Menezes,[47]
P.G. Mercadante,[3] M. Merkin,[33] A. Meyer,[18] J. Meyer[i],[20] F. Miconi,[16] N.K. Mondal,[25] M. Mulhearn,[73] E. Nagy,[12]
M. Narain,[69] R. Nayyar,[42] H.A. Neal,[56] J.P. Negret,[5] P. Neustroev,[35] H.T. Nguyen,[73] T. Nunnemann,[22]
D. Orbaker,[63] J. Orduna,[72] N. Osman,[12] J. Osta,[51] A. Pal,[70] N. Parashar,[50] V. Parihar,[69] S.K. Park,[27]
R. Partridge[e],[69] N. Parua,[49] A. Patwa[j],[65] B. Penning,[45] M. Perfilov,[33] Y. Peters,[41] K. Petridis,[41] G. Petrillo,[63]
P. Pétroff,[13] M.-A. Pleier,[65] V.M. Podstavkov,[45] A.V. Popov,[34] M. Prewitt,[72] D. Price,[41] N. Prokopenko,[34]
J. Qian,[56] A. Quadt,[20] B. Quinn,[58] P.N. Ratoff,[39] I. Razumov,[34] I. Ripp-Baudot,[16] F. Rizatdinova,[68]
M. Rominsky,[45] A. Ross,[39] C. Royon,[15] P. Rubinov,[45] R. Ruchti,[51] G. Sajot,[11] A. Sánchez-Hernández,[28]
M.P. Sanders,[22] A.S. Santos[h],[1] G. Savage,[45] L. Sawyer,[54] T. Scanlon,[40] R.D. Schamberger,[64] Y. Scheglov,[35]
H. Schellman,[48] C. Schwanenberger,[41] R. Schwienhorst,[57] J. Sekaric,[53] H. Severini,[67] E. Shabalina,[20] V. Shary,[15]
S. Shaw,[57] A.A. Shchukin,[34] V. Simak,[7] P. Skubic,[67] P. Slattery,[63] D. Smirnov,[51] G.R. Snow,[59] J. Snow,[66]
S. Snyder,[65] S. Söldner-Rembold,[41] L. Sonnenschein,[18] K. Soustruznik,[6] J. Stark,[11] D.A. Stoyanova,[34] M. Strauss,[67]
L. Suter,[41] P. Svoisky,[67] M. Titov,[15] V.V. Tokmenin,[31] Y.-T. Tsai,[63] D. Tsybychev,[64] B. Tuchming,[15] C. Tully,[61]
L. Uvarov,[35] S. Uvarov,[35] S. Uzunyan,[47] R. Van Kooten,[49] W.M. van Leeuwen,[29] N. Varelas,[46] E.W. Varnes,[42]
I.A. Vasilyev,[34] A.Y. Verkheev,[31] L.S. Vertogradov,[31] M. Verzocchi,[45] M. Vesterinen,[41] D. Vilanova,[15] P. Vokac,[7]
H.D. Wahl,[44] M.H.L.S. Wang,[45] J. Warchol,[51] G. Watts,[74] M. Wayne,[51] J. Weichert,[21] L. Welty-Rieger,[48]
M.R.J. Williams,[49] G.W. Wilson,[53] M. Wobisch,[54] D.R. Wood,[55] T.R. Wyatt,[41] Y. Xie,[45] R. Yamada,[45]

S. Yang,[4] T. Yasuda,[45] Y.A. Yatsunenko,[31] W. Ye,[64] Z. Ye,[45] H. Yin,[45] K. Yip,[65] S.W. Youn,[45] J.M. Yu,[56] J. Zennamo,[62] T.G. Zhao,[41] B. Zhou,[56] J. Zhu,[56] M. Zielinski,[63] D. Zieminska,[49] and L. Zivkovic[14]

(The D0 Collaboration[*])

[1]LAFEX, Centro Brasileiro de Pesquisas Físicas, Rio de Janeiro, Brazil
[2]Universidade do Estado do Rio de Janeiro, Rio de Janeiro, Brazil
[3]Universidade Federal do ABC, Santo André, Brazil
[4]University of Science and Technology of China, Hefei, People's Republic of China
[5]Universidad de los Andes, Bogotá, Colombia
[6]Charles University, Faculty of Mathematics and Physics,
Center for Particle Physics, Prague, Czech Republic
[7]Czech Technical University in Prague, Prague, Czech Republic
[8]Institute of Physics, Academy of Sciences of the Czech Republic, Prague, Czech Republic
[9]Universidad San Francisco de Quito, Quito, Ecuador
[10]LPC, Université Blaise Pascal, CNRS/IN2P3, Clermont, France
[11]LPSC, Université Joseph Fourier Grenoble 1, CNRS/IN2P3,
Institut National Polytechnique de Grenoble, Grenoble, France
[12]CPPM, Aix-Marseille Université, CNRS/IN2P3, Marseille, France
[13]LAL, Université Paris-Sud, CNRS/IN2P3, Orsay, France
[14]LPNHE, Universités Paris VI and VII, CNRS/IN2P3, Paris, France
[15]CEA, Irfu, SPP, Saclay, France
[16]IPHC, Université de Strasbourg, CNRS/IN2P3, Strasbourg, France
[17]IPNL, Université Lyon 1, CNRS/IN2P3, Villeurbanne, France and Université de Lyon, Lyon, France
[18]III. Physikalisches Institut A, RWTH Aachen University, Aachen, Germany
[19]Physikalisches Institut, Universität Freiburg, Freiburg, Germany
[20]II. Physikalisches Institut, Georg-August-Universität Göttingen, Göttingen, Germany
[21]Institut für Physik, Universität Mainz, Mainz, Germany
[22]Ludwig-Maximilians-Universität München, München, Germany
[23]Panjab University, Chandigarh, India
[24]Delhi University, Delhi, India
[25]Tata Institute of Fundamental Research, Mumbai, India
[26]University College Dublin, Dublin, Ireland
[27]Korea Detector Laboratory, Korea University, Seoul, Korea
[28]CINVESTAV, Mexico City, Mexico
[29]Nikhef, Science Park, Amsterdam, the Netherlands
[30]Radboud University Nijmegen, Nijmegen, the Netherlands
[31]Joint Institute for Nuclear Research, Dubna, Russia
[32]Institute for Theoretical and Experimental Physics, Moscow, Russia
[33]Moscow State University, Moscow, Russia
[34]Institute for High Energy Physics, Protvino, Russia
[35]Petersburg Nuclear Physics Institute, St. Petersburg, Russia
[36]Institució Catalana de Recerca i Estudis Avançats (ICREA) and Institut de Física d'Altes Energies (IFAE), Barcelona, Spain
[37]Uppsala University, Uppsala, Sweden
[38]Taras Shevchenko National University of Kyiv, Kiev, Ukraine
[39]Lancaster University, Lancaster LA1 4YB, United Kingdom
[40]Imperial College London, London SW7 2AZ, United Kingdom
[41]The University of Manchester, Manchester M13 9PL, United Kingdom
[42]University of Arizona, Tucson, Arizona 85721, USA
[43]University of California Riverside, Riverside, California 92521, USA
[44]Florida State University, Tallahassee, Florida 32306, USA
[45]Fermi National Accelerator Laboratory, Batavia, Illinois 60510, USA
[46]University of Illinois at Chicago, Chicago, Illinois 60607, USA
[47]Northern Illinois University, DeKalb, Illinois 60115, USA
[48]Northwestern University, Evanston, Illinois 60208, USA
[49]Indiana University, Bloomington, Indiana 47405, USA
[50]Purdue University Calumet, Hammond, Indiana 46323, USA
[51]University of Notre Dame, Notre Dame, Indiana 46556, USA
[52]Iowa State University, Ames, Iowa 50011, USA
[53]University of Kansas, Lawrence, Kansas 66045, USA
[54]Louisiana Tech University, Ruston, Louisiana 71272, USA
[55]Northeastern University, Boston, Massachusetts 02115, USA
[56]University of Michigan, Ann Arbor, Michigan 48109, USA
[57]Michigan State University, East Lansing, Michigan 48824, USA
[58]University of Mississippi, University, Mississippi 38677, USA

[59] *University of Nebraska, Lincoln, Nebraska 68588, USA*
[60] *Rutgers University, Piscataway, New Jersey 08855, USA*
[61] *Princeton University, Princeton, New Jersey 08544, USA*
[62] *State University of New York, Buffalo, New York 14260, USA*
[63] *University of Rochester, Rochester, New York 14627, USA*
[64] *State University of New York, Stony Brook, New York 11794, USA*
[65] *Brookhaven National Laboratory, Upton, New York 11973, USA*
[66] *Langston University, Langston, Oklahoma 73050, USA*
[67] *University of Oklahoma, Norman, Oklahoma 73019, USA*
[68] *Oklahoma State University, Stillwater, Oklahoma 74078, USA*
[69] *Brown University, Providence, Rhode Island 02912, USA*
[70] *University of Texas, Arlington, Texas 76019, USA*
[71] *Southern Methodist University, Dallas, Texas 75275, USA*
[72] *Rice University, Houston, Texas 77005, USA*
[73] *University of Virginia, Charlottesville, Virginia 22904, USA*
[74] *University of Washington, Seattle, Washington 98195, USA*

We present measurements of the forward-backward asymmetry in the angular distribution of leptons from decays of top quarks and antiquarks produced in proton-antiproton collisions. We consider the final state containing a lepton and at least three jets. The entire sample of data collected by the D0 experiment during Run II of the Fermilab Tevatron Collider, corresponding to $9.7\,\mathrm{fb}^{-1}$ of integrated luminosity, is used. The asymmetry measured for reconstructed leptons is $A_{\mathrm{FB}}^l = \left(2.9 \pm 2.1\,(\mathrm{stat.})^{+1.5}_{-1.7}\,(\mathrm{syst.})\right)\%$. When corrected for efficiency and resolution effects within the lepton rapidity coverage of $|y_l| < 1.5$, the asymmetry is found to be $A_{\mathrm{FB}}^l = \left(4.2 \pm 2.3\,(\mathrm{stat.})^{+1.7}_{-2.0}\,(\mathrm{syst.})\right)\%$. We examine the dependence of A_{FB}^l on the transverse momentum and rapidity of the lepton. Combination with the asymmetry measured in the final states containing two leptons yields $A_{\mathrm{FB}}^l = \left(4.2 \pm 2.0\,(\mathrm{stat.}) \pm 1.4\,(\mathrm{syst.})\right)\%$. The results are in agreement with predictions from the next-to-leading-order QCD generator MC@NLO, which predicts an asymmetry of $A_{\mathrm{FB}}^l = 2.0\%$ for $|y_l| < 1.5$.

PACS numbers: 14.65.Ha,12.38.Qk,11.30.Er,13.85.-t

I. INTRODUCTION

Within the standard model of particle physics (SM), top quarks are usually produced via quantum chromodynamic (QCD) interactions in quark-antiquark pairs. The process $p\bar{p} \to t\bar{t}(X)$ is predicted to produce mostly events for which the rapidity of the top quark, y_t, is greater than the rapidity of the top antiquark, $y_{\bar{t}}$. The rapidity y is defined as $y(\theta, \beta) = \frac{1}{2} \ln\left[(1 + \beta\cos\theta)/(1 - \beta\cos\theta)\right]$, where θ is the polar angle and β is the ratio of a particle's momentum to its energy. The angle $\theta = 0$ corresponds to the direction of the incoming proton. This predicted forward-backward asymmetry is mostly due to contributions at order α_s^3, where α_s is the QCD coupling constant [1]. There are also smaller contributions to the forward-backward asymmetry from electroweak (EW) interactions [2]. Forward-backward asymmetries in $p\bar{p} \to t\bar{t}(X)$ production previously measured at the Fermilab Tevatron Collider [3–5] were found to be somewhat higher than the SM predictions [6, 7]. With a mass of approximately $173\,\mathrm{GeV}$ [8], the top quark is the most massive known elementary particle, which raises the possibility that the asymmetry is enhanced by effects beyond the SM. Hence, the previously measured asymmetries led to studies of possible causes not only within, but also beyond the SM [9].

Top quarks decay almost exclusively into a b quark and a W boson, and W bosons decay either hadronically to a quark and an antiquark or leptonically to a lepton and a neutrino. Thus, $t\bar{t}$ events are usually classified based on the number of leptons from the decays of the W bosons into the dilepton, lepton+jets (l+jets), and all-jets channels. The $t\bar{t}$ production asymmetry was first measured by the D0 Collaboration [10] in the l+jets channel. The result of Ref. [10] was superseded by that of Ref. [3], where a dataset corresponding to an integrated luminosity of $5.4\,\mathrm{fb}^{-1}$ was used to measure an inclusive asymmetry of $\left(20^{+6}_{-7}\right)\%$. The CDF Collaboration measured this asymmetry in the l+jets channel with $9.4\,\mathrm{fb}^{-1}$ of integrated luminosity, finding $A_{\mathrm{FB}} = (16.4 \pm 4.5)\%$ [5]. These measured values can be compared to SM predictions, for example, $A_{\mathrm{FB}} = (8.8 \pm 0.9)\%$ [6].

*with visitors from [a]Augustana College, Sioux Falls, SD, USA, [b]The University of Liverpool, Liverpool, UK, [c]DESY, Hamburg, Germany, [d]Universidad Michoacana de San Nicolas de Hidalgo, Morelia, Mexico [e]SLAC, Menlo Park, CA, USA, [f]University College London, London, UK, [g]Centro de Investigacion en Computacion - IPN, Mexico City, Mexico, [h]Universidade Estadual Paulista, São Paulo, Brazil, [i]Karlsruher Institut für Technologie (KIT) - Steinbuch Centre for Computing (SCC), D-76128 Karlsrue, Germany, [j]Office of Science, U.S. Department of Energy, Washington, D.C. 20585, USA, [k]American Association for the Advancement of Science, Washington, D.C. 20005, USA [l]Kiev Institute for Nuclear Research, Kiev, Ukraine and [m]Laboratoire de Physique Theorique, Orsay, FR.

The forward-backward asymmetry in the production of $t\bar{t}$ pairs leads to a forward-backward asymmetry A_{FB}^{l} in the angular distribution of the leptons produced in the $t\bar{t}$ decays [11]. The asymmetry A_{FB}^{l} was first measured by D0 [3] as a cross-check of the asymmetry of the $t\bar{t}$ pair and to demonstrate that the observed tension with the SM should not be attributed to biases introduced by the algorithm used to reconstruct the $t\bar{t}$ system or to the corrections for the detector acceptance and resolution effects. In SM $p\bar{p} \rightarrow t\bar{t}(X)$ production, the polarization of top quarks is negligible and the leptons are produced isotropically (in the appropriate reference frames) leading to an A_{FB}^{l} that is smaller than A_{FB}. The D0 Collaboration measured $A_{\mathrm{FB}}^{l} = (15.2 \pm 4.0)\%$ in the l+jets channel for $|y_l| < 1.5$, where y_l is the rapidity of the lepton from top quark decay [3] and $A_{\mathrm{FB}}^{l} = (5.8 \pm 5.3)\%$ in the dilepton channel for $|y_l| < 2$ [12]. The CDF Collaboration measured this asymmetry in the l+jets channel and found values extrapolated to the full acceptance of $A_{\mathrm{FB}}^{l} = (9.4_{-2.9}^{+3.2})\%$ [13]. The corresponding SM predictions range from 2.0% to 3.8% [6, 14, 15]. The higher predictions include electroweak corrections, which increase A_{FB}^{l} by less than a percent (absolute). The dominant uncertainty on these predictions is from the renormalization and factorization scales, and is evaluated to be up to 1.0% [6, 15]. The results of the previous measurements could be taken as an indication of effects beyond the SM that lead to the production of polarized top quarks [16]. Motivated by the desire to further investigate this tension and by the potential sensitivity of A_{FB}^{l} to new physics, we pursue this analysis in greater detail and with a larger dataset.

Measuring the leptonic asymmetry rather than the $t\bar{t}$ asymmetry has additional benefits. The measurements of the $t\bar{t}$ asymmetry require full reconstruction of the $t\bar{t}$ decay chain, accomplished by assuming on-shell top quarks that each decay to three final state fermions. These assumptions limit the validity of a comparison of data to calculations that include higher orders in top quark decay and off-shell top quarks (e.g., in loops). These limitations are not intrinsic to the lepton-based asymmetry. Although we make some use of $t\bar{t}$ reconstruction, the effects of off-shell top quarks and of decays with additional final-state partons on the measurement of A_{FB}^{l} are negligible.

Experimentally, the direction of a lepton is determined with far greater precision than that of a top quark. Thus, corrections for the detector acceptance and experimental resolutions are simpler. Furthermore, with no need for full reconstruction of the $t\bar{t}$ system, the l+3 jet sample can be used for this measurement in addition to the previously used $l{+}{\geq}4$ jets sample. This addition almost doubles the number of $t\bar{t}$ events analyzed, at the expense of a lower signal-to-background ratio. The inclusion of the l+3 jet sample also reduces the acceptance corrections (see Section VI), which are a leading source of systematic uncertainty in Ref. [3].

In Ref. [5], the CDF Collaboration reported a strong

increase of A_{FB} with the invariant mass of the $t\bar{t}$ system, $m_{t\bar{t}}$. The dependence of the asymmetry on $m_{t\bar{t}}$ observed in the previous D0 measurement [3] is statistically consistent with both the SM prediction and the CDF result. Measuring $m_{t\bar{t}}$ requires full reconstruction of the $t\bar{t}$ system, but we can also study the dependence of the asymmetry on the $t\bar{t}$ kinematics by relying on the transverse momentum of the lepton, p_T^l. This observable can readily be studied in l+3 jet events and is measured with far greater precision than $m_{t\bar{t}}$. Furthermore, p_T^l is strongly correlated with $m_{t\bar{t}}$, and is useful in comparing data to the predictions of different models [17]. This differential measurement is therefore well motivated both experimentally and as a test of new physics models.

We report here an updated measurement of A_{FB}^{l}, using the full dataset collected from 2002 to 2011 by the D0 experiment during Run II of the Fermilab Tevatron Collider at $\sqrt{s} = 1.96\,\mathrm{TeV}$. We extend the measurement to include l+3 jet events, which required improvements in the background modeling, and measure the p_T^l dependence of A_{FB}^{l} for the first time. The measurement reported in this paper supersedes the results of Ref. [3].

II. THE D0 DETECTOR

The D0 coordinate system has the z axis along the direction of the proton beam. The distribution of the $p\bar{p}$ collisions in the z direction is roughly Gaussian, with a width of 25 cm. Particle directions are presented in terms of their azimuthal angle ϕ and their rapidity y or their pseudorapidity $\eta = -\ln\left[\tan\left(\frac{\theta}{2}\right)\right]$, where θ is the polar angle relative to the primary $p\bar{p}$ collision vertex (PV). We also use the pseudorapidity defined relative to the center of the detector, η_{det}.

The D0 detector [18] is a multipurpose particle detector, with the main components listed below. At the core is a silicon microstrip tracker [19, 20] arranged in five barrel layers and 14 disks. These include an innermost silicon layer [20] that was added in 2006, and was not present for the period of data taking that corresponds to the first $1.0\,\mathrm{fb}^{-1}$. The silicon system is followed by an eight-layer scintillating-fiber tracking system. The tracking system provides an impact parameter resolution of $18\,\mu\mathrm{m}$ in the plane transverse to the beams for tracks of particles with high transverse momentum (p_T) that are produced within the pseudorapidity region of $|\eta_{\mathrm{det}}| < 3.0$. The tracking system is located within a superconducting solenoid magnet that provides a 1.9 T axial magnetic field and is surrounded by liquid argon / uranium calorimeters.

The calorimeters [21] are enclosed within a central barrel cryostat that covers angles up to $|\eta_{\mathrm{det}}| \approx 1.1$ and two end-cap cryostats which extend the coverage to $|\eta_{\mathrm{det}}| \approx 4.2$. They consist of an electromagnetic calorimeter with a granularity of up to about $\Delta\eta \times \Delta\phi = 0.5 \times 0.5$, reached at a depth typical of electromagnetic showers, and a hadronic calorimeter with a granularity of about

$\Delta\eta \times \Delta\phi = 0.1 \times 0.1$. Plastic scintillator detectors are placed between the central and each endcap cryostat to provide additional sampling of the showers that develop at $1.1 < |\eta_{\text{det}}| < 1.4$. The calorimetry readout defines cells which are arranged in semi-projective towers, with 7–11 layers per tower, depending on η_{det}.

A muon detection system [22] surrounds the calorimetry, and consists of an iron toroidal magnet that provides a field of $1.8\,\text{T}$ and of three layers of tracking detectors and scintillation trigger detectors. The muon system provides coverage up to $|\eta_{\text{det}}| = 2$.

Data collection is triggered by a three-level system. The first trigger level uses local trigger elements implemented in hardware, such as the energy deposited within a single calorimetry tower, and has an accept rate of about $2\,\text{kHz}$. The second trigger level combined these trigger elements and reduces the event rate to about $1\,\text{kHz}$. The third trigger level is implemented by a farm of Linux-based processors which fully reconstruct the high-level objects in each event, such as jets and muons, and triggers event storage at a typical rate of $100\,\text{Hz}$.

III.   DEFINING THE LEPTON-BASED ASYMMETRY

In this analysis, we measure the charge (q_l) and rapidity (y_l) of the electron or muon that originates from the W boson from top quark decay. Events with $q_l y_l > 0$ are defined as forward and events with $q_l y_l < 0$ are defined as backward. We define the lepton-based forward-backward asymmetry as

$$A_{\text{FB}}^l = \frac{N_F^l - N_B^l}{N_F^l + N_B^l}, \qquad (1)$$

where N_F^l and N_B^l are the number of forward and backward events, respectively. All asymmetries are reported after subtracting the estimated background.

The asymmetry can be defined at the "reconstruction level," which refers to the measured lepton parameters and is affected by acceptance and resolution. To enable direct comparisons with SM and non-SM calculations, the asymmetry can also be defined at the "production level," before acceptance and resolution effects take place. The production level is sometimes also denoted as the generator level, or the parton level.

Though the rapidity coverage differs for electrons and muons, we assume lepton flavor universality and define A_{FB}^l and the acceptance in terms of $|y_l|$. To avoid large acceptance corrections, only events with $|y_l| < 1.5$ are used (see Ref. [3]). Throughout most of this paper, the production-level A_{FB}^l is defined counting only leptons produced within this lepton coverage. However, in Section XI we also discuss asymmetries extrapolated to the full acceptance.

IV.   ANALYSIS STRATEGY

The selection focuses on $t\bar{t}(X) \to W^+ b W^- \bar{b}(X)$ events in the l+jets decay mode, where one W boson decays hadronically ($\bar{q}q'$) and the other decays leptonically ($l\bar{\nu}_l$). The experimental signature of this decay mode is one isolated lepton (e or μ) with a large p_T^l, a significant imbalance in transverse momentum measured throughout the detector ($\not{E}_T$, with the letter E indicating a calorimetry-based observable) from the undetected neutrino, and jets arising from the two b quarks and from the two quarks from $W \to \bar{q}q'$ decay. We select electrons and muons, which arise either directly from the W boson decay or through an intermediate τ lepton.

A prototypical l+jets event contains four final state quarks and hence four jets. Previous measurements selected events with at least four jets. Only half of the $t\bar{t}$ events in the l+jets channel have four or more selected jets, as one of the jets may fail the selection criteria due to insufficient p_T or due to large absolute rapidity. In addition, the decay products of two of the final state partons may be clustered into a single jet.

In this measurement we also select events with three jets. The inclusion of three-jet events has the advantages of increasing the statistical power of the measurement and making the measurement less susceptible to biases from selection. However, these additional events have a lower signal-to-background ratio than the events with ≥ 4 jets. To maximize the statistical power of the purer subsets, we separate the measurement into several channels, defined by the number of jets (3 or ≥ 4) and the number of "b-tagged" jets (0, 1, or ≥ 2), that is, jets identified as likely to originate from a b quark.

We identify variables that discriminate between the $t\bar{t}$ signal and the production of W bosons in association with jets (W+jets), and combine the variables into a single discriminant D. There are separate discriminants for l+3 jet events and l+$\geq$4 jet events. We use these discriminants to estimate the number of selected $t\bar{t}$ events and their reconstruction-level A_{FB}^l (see Section VII).

The addition of three jet events increases the sensitivity of the analysis to the modeling of W+jets production, which contributes most of the selected three jet events but only a minority of the selected $\geq$4 jet events. We study and improve the modeling of A_{FB}^l in the W+jets background using a top-depleted control sample (see Section VII C).

We then correct the $q_l y_l$ distribution to the production level within the lepton coverage, and measure the production-level A_{FB}^l. Since the angular resolutions for electrons and muons are excellent, the incorrect classification of events as forward or backward is negligibly small. We therefore correct A_{FB}^l only for acceptance effects (see Section VIII).

In addition to measuring the inclusive A_{FB}^l, we also measure A_{FB}^l in three p_T^l regions: $20 \leq p_T^l < 35\,\text{GeV}$, $35 \leq p_T^l < 60\,\text{GeV}$, and $p_T^l \geq 60\,\text{GeV}$. To measure the p_T^l dependence, we first correct for migrations between

different p_T^l regions and then correct for the effects of acceptance (see Section VIII).

V. EVENT SELECTION

The event selection criteria used in this analysis are similar to those used to measure the $t\bar{t}$ production cross section in the l+jets channel [23]. In particular, we also accept events with three selected jets. The reconstruction and identification of jets, isolated leptons, and $\not{E}_T$ is described in Ref. [24].

Only jets with transverse momentum $p_T > 20\,\text{GeV}$ and $|\eta| < 2.5$ are considered for further analysis, and events are required to contain at least three such jets. The leading jet, that is the jet with the largest p_T, is also required to have $p_T > 40\,\text{GeV}$. As in Ref. [23], we minimize the effect of multiple $p\bar{p}$ collisions in the same bunch crossing by requiring that jets are vertex confirmed [25], i.e., have at least two tracks within the jet cone pointing back to the PV.

A typical decay of a b hadron occurs at a distance of the order of $1\,\text{mm}$ from the PV and results in charged tracks that are detected by the tracking system and form a displaced secondary vertex. Thus, jets that originate from a b quark can be identified by the properties of the tracks reconstructed within the jet cone, in particular by their displacement from the PV, and by the reconstruction of displaced secondary vertices. Several observables useful for identifying such jets are combined into a multivariate discriminant [26] that is used in this analysis to tag b jets by selecting jets likely to originate from a b quark among the three or four jets with the highest p_T.

The e+jets and μ+jets channels have similar event selection requirements. Only events collected with single-lepton or lepton+jet triggers are used. The criteria for selecting e+jets events are:

- one isolated electron with $p_T > 20\,\text{GeV}$, $|\eta_{\text{det}}| < 1.1$, and $|y| < 1.5$,

- $|\not{E}_T| > 20\,\text{GeV}$, and

- $\Delta\phi(e,\not{E}_T) > (2.2 - 0.045 \cdot \not{E}_T/\text{GeV})$ radians.

For μ+jets events, the criteria are:

- one isolated muon with $p_T > 20\,\text{GeV}$ and $|y| < 1.5$,

- $25\,\text{GeV} < |\not{E}_T| < 250\,\text{GeV}$, and

- $\Delta\phi(\mu,\not{E}_T) > (2.1 - 0.035 \cdot \not{E}_T/\text{GeV})$ radians.

Events with a second isolated electron or muon passing the selection are rejected. The $|\not{E}_T| < 250\,\text{GeV}$ cut suppresses events where the $\not{E}_T$ is due to a mismeasurement of the p_T of the muon, which is reconstructed from the curvature of the track of the muon. The $\Delta\phi(l,\not{E}_T)$ cuts reduces the background from QCD multijet production. Multijet events can pass the selection when a jet is misidentified as an isolated lepton. This often results in

spurious reconstructed $\not{E}_T$ along the lepton's direction. Due to the lepton p_T requirements, the differences between the lepton's rapidity and pseudorapidity are less than 2×10^{-5}. However, the lepton's η and η_{det} can differ by as much as 0.6.

In addition to the above criteria of Ref. [23], we also require that the curvature of the track associated with the lepton is well measured. This requirement, while $\approx 97\%$ efficient for leptons produced in $t\bar{t}$ decay, suffices to lower the lepton charge misidentification rate to less than one part in a thousand. It also reduces the migration of events among the three p_T^l regions.

For events with muons with $p_T > 60\,\text{GeV}$, we also require that the magnitude of the vector sum of the muon momentum and missing transverse energy is greater than $20\,\text{GeV}$. This requirement rejects events consistent with low energy muons from low energy jets that are badly reconstructed as having high p_T, leading to their misclassification as isolated leptons. Such events are part of the multijet background, but their modeling as part of that background, using the technique described in Section VII B, is problematic. To limit any possible mismodeling, we also suppress these events with additional requirements on the track associated with the muon. Leptons from signal events pass these additional requirements with $\approx 85\%$ efficiency.

The main background after this event selection is due to W+jets production. There is a smaller contribution from multijet production. Other small backgrounds from single top quark, Z+jets and diboson production are also present.

We use the MC@NLO event generator [14] combined with HERWIG showering [27] to model the behavior of $t\bar{t}$ events, and ALPGEN [28] combined with PYTHIA [29] to simulate the W+jets background. The rate of inclusive $W + c\bar{c}$ and $W + b\bar{b}$ production predicted by ALPGEN is scaled up by a factor of 1.47, so that the ratio of the heavy flavor production rate to the inclusive W+jets production rate agrees with the ratio calculated at next-to-leading-order (NLO) [23, 30]. The simulated W-boson p_T distribution is reweighted to match the product of the measured Z-boson p_T distribution from D0 data [31] and the SM ratio of the distributions of the W-boson p_T and the Z-boson p_T, as calculated at NLO with RESBOS [32]. For the other backgrounds, Z+jets events are simulated with ALPGEN, diboson events are simulated with PYTHIA and events from single top quark production are simulated with COMPHEP [33]. The normalizations for the last three background processes are taken from NLO calculations [30]. For all simulated events, event generation is followed by the D0 detector simulation and reconstruction programs. To model energy depositions from noise and additional $p\bar{p}$ collisions within the same bunch crossing, simulated events are overlaid with data from random $p\bar{p}$ crossings. The properties of the multijet background are evaluated using control samples from collider data.

VI. THE PREDICTED ASYMMETRIES

As the asymmetry first appears at order α_s^3, with the largest contribution due to a loop diagram, it is not fully simulated by tree-level event generators such as PYTHIA or ALPGEN. In addition, the modeling of selection and reconstruction effects requires full Monte Carlo (MC) simulation. The MC@NLO event generator is well suited for this measurement as it couples a NLO calculation of $t\bar{t}$ production with subsequent parton showers to fully simulate $t\bar{t}$ events. The asymmetries of simulated $t\bar{t}$ and W+jets production are listed in Table I for different jet and b-tag multiplicities.

The two leading contributions to the $t\bar{t}$ asymmetry, at order α_s^3, are as follows [1]. In events with no additional radiated partons, the interference between the Born and box diagrams leads to a positive asymmetry. At order α_s^3, the p_T of the $t\bar{t}$ system for these events is $p_T^{t\bar{t}} = 0$. However, realistic simulation of these processes using parton showers allows for some transverse boost of the $t\bar{t}$ system. The interference between diagrams containing initial or final state radiation decreases the asymmetry. These events have non-zero $p_T^{t\bar{t}}$ at order α_s^3, and $p_T^{t\bar{t}}$ is usually increased by the parton showers. Thus the predicted asymmetry decreases as a function of $p_T^{t\bar{t}}$, as shown in Fig. 1a, which can also be seen in Table I as a decrease in $A_{\rm FB}^l$ with increasing jet multiplicity. The dependence on the number of b tags follows the same pattern, with the ≥ 4 jet, 0 tag channel having the hardest $p_T^{t\bar{t}}$ spectrum and the 3 jet, ≥ 2 tag channel having the softest $p_T^{t\bar{t}}$ spectrum. The inclusion of three-jet events reduces the dependence of the acceptance on $p_T^{t\bar{t}}$, as shown in Fig. 1b.

In the case of W+jets background production, W bosons produced by interactions involving gluons or sea quarks contribute positively to the asymmetry. On the other hand, W bosons produced by valence-valence collisions contribute negatively to the overall asymmetry. The production of W bosons in association with heavy flavor quarks occurs predominantly due to valence–valence collisions, and thus has a lower $A_{\rm FB}^l$ compared to inclusive W-boson production, as seen in Table I.

TABLE I: Simulated reconstructed asymmetries for selected $t\bar{t}$ and W+jets events, by event category. The quoted uncertainties are due to the finite sizes of the simulated samples.

	$A_{\rm FB}^l$, %	
Channel	$t\bar{t}$ signal	W+jets background
l+jets, all channels	1.6 ± 0.1	13.0 ± 0.2
l+3 jets, 0 b tags	2.3 ± 0.3	13.5 ± 0.3
l+3 jets, 1 b tag	2.7 ± 0.3	11.6 ± 0.4
l+3 jets, ≥ 2 b tags	2.8 ± 0.2	7.4 ± 0.9
l+≥ 4 jets, 0 b tags	-0.9 ± 0.4	14.1 ± 0.9
l+≥ 4 jets, 1 b tag	0.5 ± 0.2	14.5 ± 1.0
l+≥ 4 jets, ≥ 2 b tags	1.1 ± 0.2	8.8 ± 1.9

VII. MEASURING THE RECONSTRUCTED $A_{\rm FB}^l$

We construct a discriminant (see Section VII A), and extract the sample composition and the asymmetry using a maximum likelihood fit to the distribution of the discriminant and the distribution of the sign of $q_l y_l$ (see Section VII B). The asymmetry values measured at this stage rely on the simulated asymmetry of the W+jets background. We then use the estimated sample composition to derive weights for the simulated W+jets background that are based on the asymmetry of control data, as described in Section VII C. We apply this reweighting, which does not affect the estimation of the sample composition, and repeat the maximum likelihood fit to measure the reconstructed $A_{\rm FB}^l$ for $t\bar{t}$ events.

A. The discriminant

We choose input variables that (a) provide good separation between $t\bar{t}$ signal and W+jets production, (b) are well modeled, (c) have little correlation with y_l, q_l, and p_T^l, and (d) are not strongly correlated between themselves (the correlation factors of all but one pairing are below 0.3). We combine the input variables to form a discriminant D (as in Refs. [10, 34]) based on the approximate likelihood ratio between the $t\bar{t}$ and W+jets hypotheses. The correlations between the input variables are not exploited in D, which is constructed using only the simulated one-dimensional distributions of these variables.

For the $l+\geq 4$ jet channels, D is constructed exactly as in Ref [3]. We first reconstruct the full $t\bar{t}$ decay chain using a constrained kinematic fit algorithm [35]. For each assignment of the four leading jets to the four quarks from $t\bar{t}$ decay, the algorithm scales the four-momenta of the observed objects to minimize a χ^2 test statistic. The χ^2 test statistic measures the consistency of the scaled four-momenta with the constraints imposed by the known W boson and top quark masses, given the experimental resolutions. Only assignments that are consistent with the observed b tags are considered. The most likely assignment and the scaled four-momenta that minimize χ^2 are used to reconstruct the W-boson and top-quark resonances. We then build the discriminant from the following variables:

- χ^2 of the likeliest assignment. Low values indicate a $t\bar{t}$ event.

- $p_T^{\rm LB}$, the transverse momentum of the leading b-tagged jet, or when no jets are b tagged, the p_T of the leading jet. Values below $p_T^{\rm LB} \approx 50\,{\rm GeV}$ are indicative of W+jets production.

- $k_T^{\rm min} = \min\left(p_{T,a}, p_{T,b}\right) \cdot \Delta\mathcal{R}_{ab}$, where $\Delta\mathcal{R}_{ab} = \sqrt{(\eta_a - \eta_b)^2 + (\phi_a - \phi_b)^2}$ is the angular distance
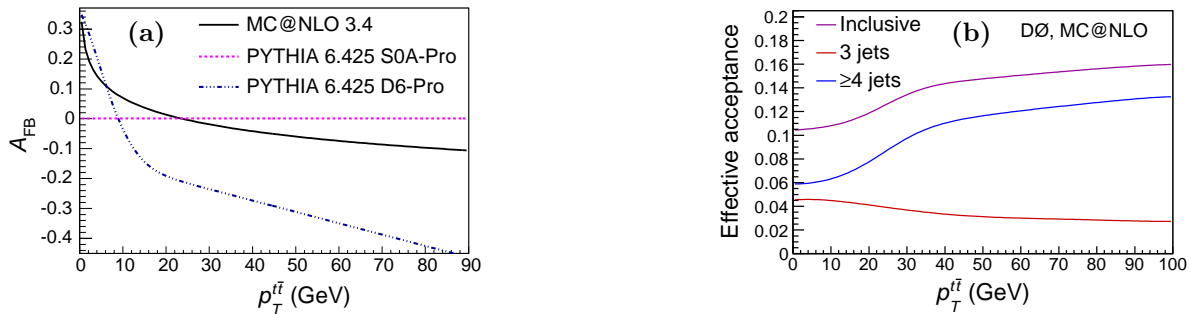
FIG. 1: The dependence of (a) the $t\bar{t}$ asymmetry and (b) the effective acceptance on $p_T^{t\bar{t}}$. Figure (a) is adapted from Ref. [3], and the simulated predictions were studied in further detail in Ref. [36]. Figure (b) shows the effective acceptance, which accounts for the channel weights introduced below in Section VIII.

between the two closest jets, a and b, and $p_{T,a}$ and $p_{T,b}$ are their transverse momenta.

- M_{jj}, the invariant mass of the jets assigned to the $W \to q\bar{q}'$ decay in the kinematic fit, calculated using kinematic quantities before the fit.

Of these variables, only χ^2 depends on the lepton, and that dependence is small as it also depends on the kinematics of the four leading jets. Thus, this discriminant has little correlation with p_T^l and $q_l y_l$.

The variables χ^2 and M_{jj} are based on the full $t\bar{t}$ reconstruction, so for the $l+3$ jet channels we construct a different discriminant. It is constructed in the same manner, but with the following variables:

- S, the sphericity, defined as $S = \frac{3}{2}(\lambda_2 + \lambda_3)$, where λ_2 and λ_3 are the largest two out of the three eigenvalues of the normalized quadratic momentum tensor M. The tensor M is defined as

$$M_{ij} = \frac{\sum_o p_i^o p_j^o}{\sum_o |p^o|^2}, \qquad (2)$$

where p^o is the momentum vector of a reconstructed object o, and i and j are the three Cartesian coordinates. The sum over objects includes the three selected jets and the selected charged lepton. Due to the high mass of the top quarks, $t\bar{t}$ events tend to be more spherical than background events.

- p_T^{3rd}, the transverse momentum of the third leading jet. This variable tends to have higher values for signal than for background.

- M_{jj}^{min}, the lowest of the invariant masses of two jets, out of the three possible jet pairings. The simulation of this variable in W+jets production is discussed in Section IX.

- p_T^{LB}, defined as for the $l+{\geq}4$ jet channel, above.

- $\Delta\phi(\text{jet}_1, \not{E}_T)$, the difference in azimuthal angle between the leading jet and the transverse momentum imbalance. This variable provides additional discrimination between the multijet background and signal. In multijet events the missing energy often originates from jet energy mismeasurement and therefore tends to be directed opposite to the direction of the leading jet, whereas in $t\bar{t}$ events the missing energy is generated by an escaping neutrino.

Jets that arise from gluon splitting are typical of W+jets and multijet production, and tend to have a low invariant mass and somewhat lower p_T than jets in $t\bar{t}$ events. Thus, low M_{jj}^{min}, M_{jj}, and k_T^{min} values are indicative of background.

The distributions of these variables in data and their modeling are shown in Fig. 2 for $l+{\geq}4$ jet events and in Fig. 3 for $l+3$ jet events. The fractions of $t\bar{t}$ signal, W+jets background and multijet background are taken from the results of the fit described in the next subsection. The number of events (N_{OB}) due to the other background processes, Z+jets, single top quark and diboson production, is fixed to the predicted value.

B. Maximum likelihood fit

Selected events are categorized into six channels by the number of jets and b tags. The $l+3$ jet, zero-b-tag channel serves as a control region for the asymmetries of the W+jets background while the other five "signal" channels are used in the maximum likelihood fit. The number of selected $t\bar{t}$, W+jets, and multijet events in the five signal channels, i.e., the sample composition of the data sample, and the reconstructed A_{FB}^l are extracted simultaneously using a maximum likelihood fit to the distributions of D and $\text{sgn}(q_l y_l)$ (the sgn function is 1 if its operand is positive and -1 otherwise) across the five signal channels. The distribution of the discriminant across all channels is shown in Fig. 4. The following four samples are used to construct the templates for the fit:

- simulated $t\bar{t}$ signal events with $q_l y_l > 0$,

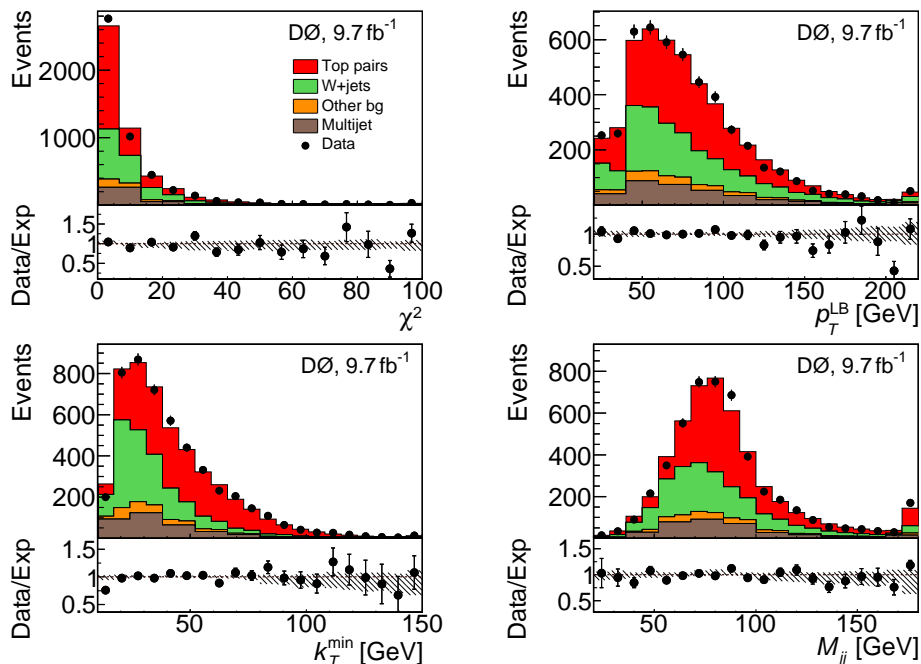- simulated $t\bar{t}$ signal events with $q_l y_l < 0$,

FIG. 2: Input variables to the discriminant in the $l+\geq 4$ jets sample (see Section VII A for definitions of variables). Overflows are shown in the extreme bins. The ratios between the data counts and the model expectations are shown in the lower panel of each figure. The hashed area indicates the systematic uncertainties on the model expectations.

- simulated W+jets events,

- a control data sample that has been enriched in multijet production by inverting the lepton isolation requirements [23].

The shape of the discriminant is the same for both signal templates. Thus, their relative contribution is controlled by the $\text{sgn}(q_l y_l)$ distribution, which yields the fitted reconstruction-level asymmetry, after background subtraction.

The normalization of the multijet background is determined using the observed number of events in the multijet-enriched control sample and the probability of a jet to satisfy the lepton quality requirements [23]. The probability for jets to pass lepton quality requirements, particularly in the μ+jets channel, is dependent on p_T^l. We therefore split the multijet background template into six components, one for each lepton flavor and p_T^l region. The presence of signal in the multijet control sample ("signal contamination") is accounted for both in the likelihood and when calculating the relative weights of the templates in the data model (e.g., in Figs. 2 and 3). To reduce statistical fluctuations in the p_T^l-dependent measurement, and in other fits of subsamples (see Section X), the number of bins of the multijet discriminant distributions is reduced by a factor of two, and for the $p_T^l \geq 60$ GeV measurement, by a factor of three.

The results of this fit are given in Table II, where the measured A_{FB}^l values are from the fit done after the reweighting of the W+jets background described below. We also list a breakdown of the sample composition by

channel in Table III, this breakdown is not used in the analysis. In Fig. 5, the distributions of $q_l y_l$ are taken from the simulated samples, with the exception of the distribution for multijet production, which is modeled from the multijet-enriched control sample. The distribution for W+jets is shown after the reweighting described in the next section.

TABLE II: Predicted and measured A_{FB}^l values at reconstruction level, numbers of events estimated from signal and background sources, and total numbers of events selected, excluding the three-jet zero-b-tag control data. The quoted uncertainties on the measured values are statistical. The MC@NLO predictions are listed with their total uncertainties.

| Quantity | p_T^l range, GeV | | | |
	≥ 20	20–35	35–60	≥ 60
Pred. A_{FB}^l, %	1.6 ± 0.2	1.2 ± 0.5	1.2 ± 0.4	2.3 ± 0.3
A_{FB}^l, %	2.9 ± 2.1	-1.2 ± 4.1	3.0 ± 3.2	7.2 ± 3.6
$N_{W+\text{jets}}$	4445 ± 68	1609 ± 40	1842 ± 45	1008 ± 41
N_{multijet}	969 ± 23	325 ± 13	309 ± 14	333 ± 14
N_{OB}	787	271	319	197
$N_{t\bar{t}}$	4746 ± 64	1341 ± 38	1951 ± 43	1438 ± 38
N_{sel}	10947	3548	4422	2977

C. Reweighting the simulated W+jets background

Since both the W+jets background and the $t\bar{t}$ signal contribute to the A_{FB}^l of the selected data, accurate mod-
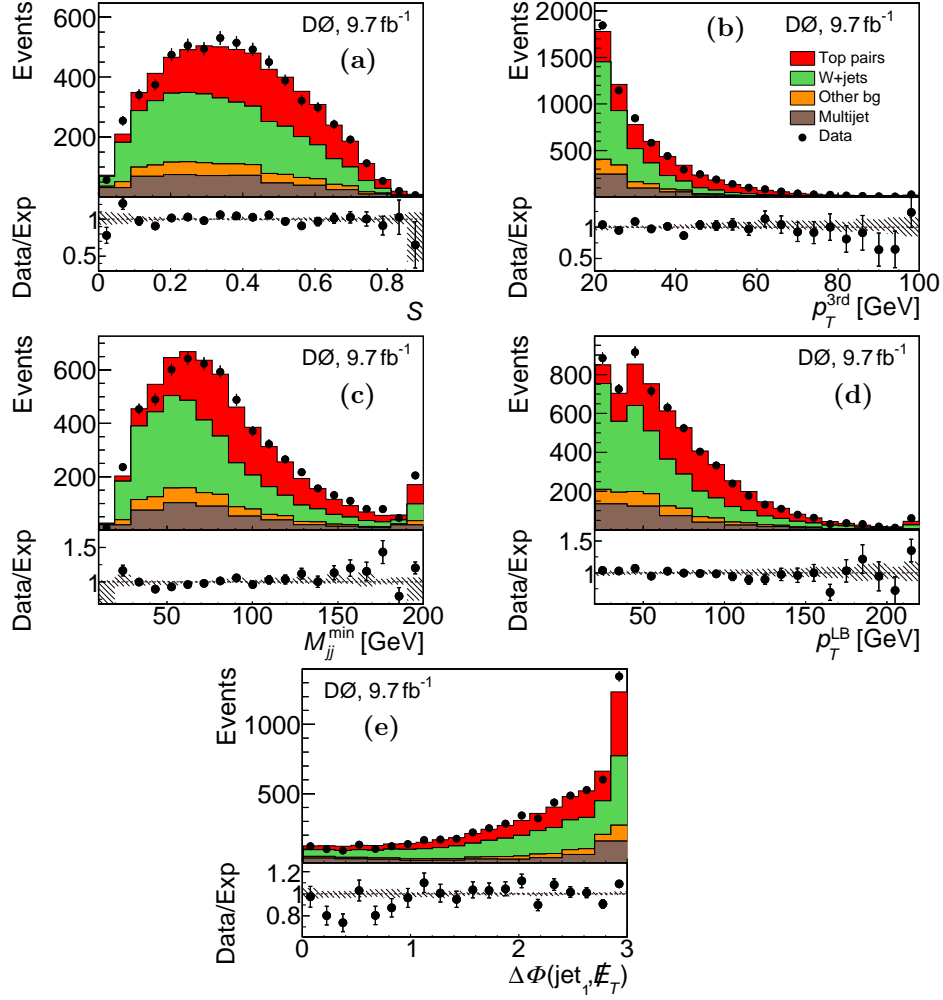
FIG. 3: Input variables to the discriminant in the l+3 jet sample (see Section VII A for definitions of variables) for events with at least one b tag. Overflows are shown in the extreme bins. The ratios between the data counts and the model expectations are shown in the lower panel of each figure. The hashed area indicates the systematic uncertainties on the model expectations.
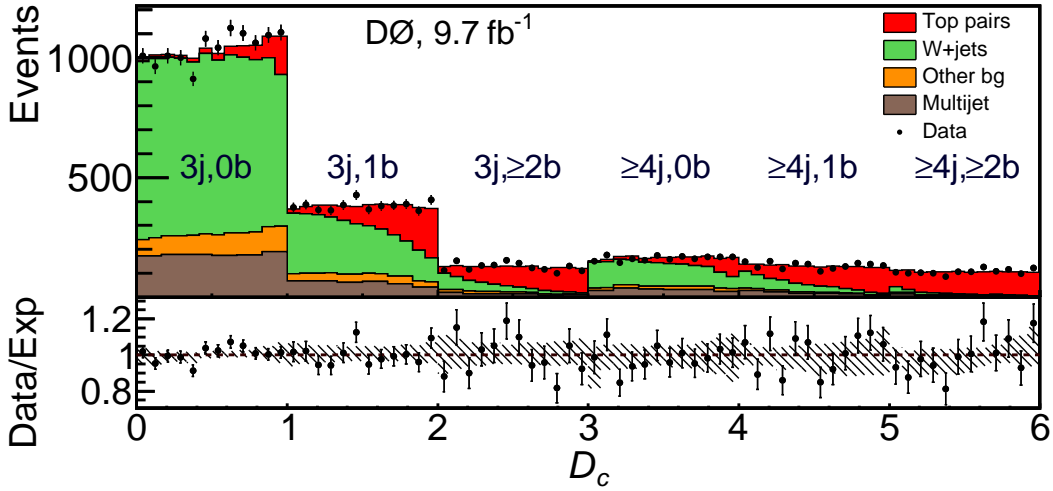

FIG. 4: The discriminants for all channels, concatenated into a single variable D_c. Each unit of D_c corresponds to a channel, as labeled in the plot. The region $D_c < 1$ is not used in the fit for sample composition and A_{FB}^l. The ratio of the data counts and the model expectation is shown below. The hashed area indicates the systematic uncertainties on the model expectations.

TABLE III: Breakdown by channel of the composition of the inclusive ($p_T^l \geq 20$) sample. See Table II for the fit uncertainties. The last two rows list the predicted and observed number of events in each channel.

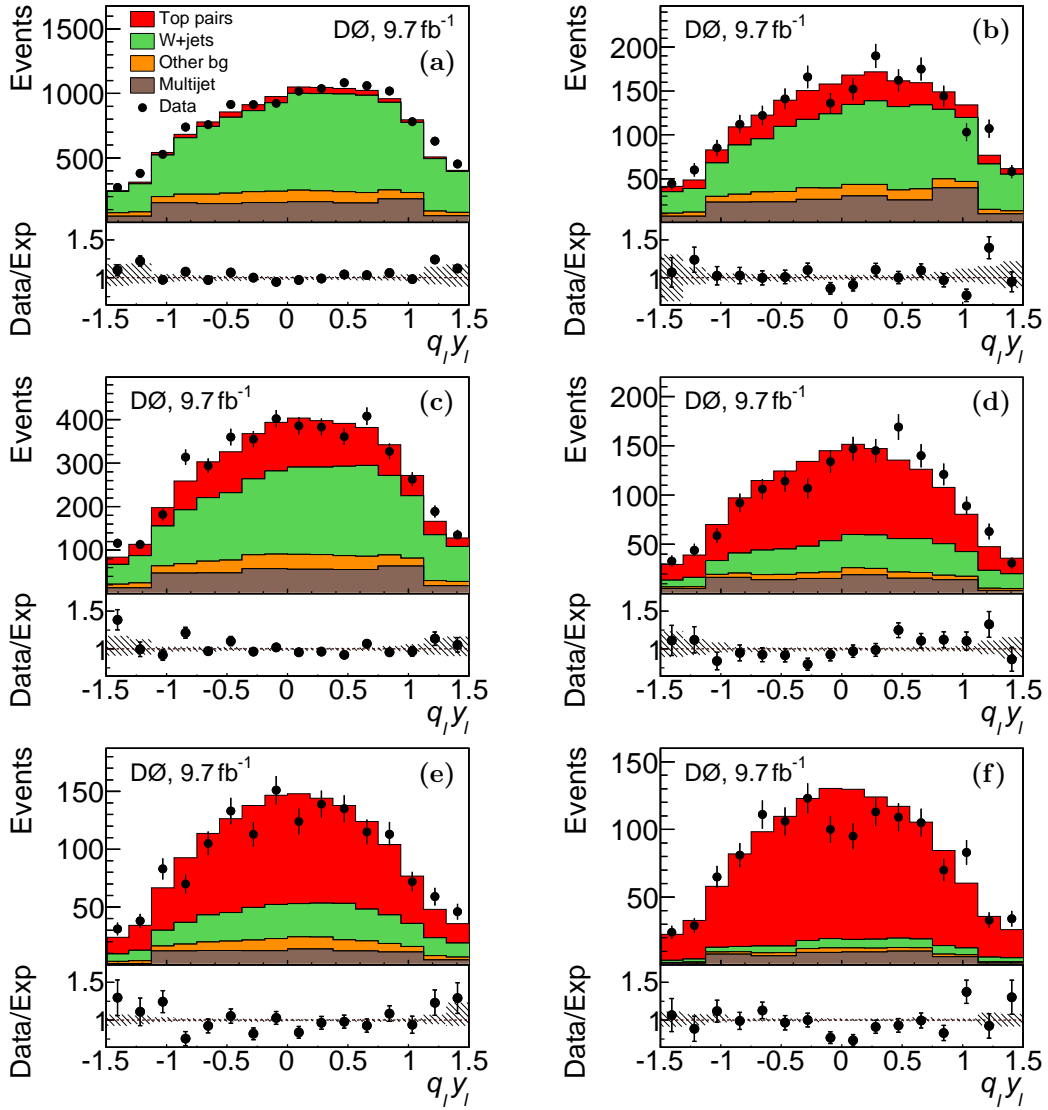| | $l+3$ jets | | | $l+\geq 4$ jets | | |
	0 b tags	1 b tag	≥ 2 b tags	0 b tags	1 b tag	≥ 2 b tags
$N_{W+\text{jets}}$	9167	2461	352	1151	403	79
N_{multijet}	1325	449	95	236	127	62
N_{OB}	1117	404	112	163	75	33
$N_{t\bar{t}}$	535	1212	1001	383	983	1166
Sum	12145	4527	1560	1933	1588	1339
N_{sel}	12509	4588	1527	1957	1594	1281

FIG. 5: The $q_l y_l$ distribution for: (a) $l+3$ jets and 0 b tags, (b) $l+\geq 4$ jets and 0 b tags, (c) $l+3$ jets and 1 b tag, (d) $l+\geq 4$ jets and 1 b tag, (e) $l+3$ jets and ≥ 2 b tags, and (f) $l+\geq 4$ jets and ≥ 2 b tags. The ratio between the data counts and the model expectation is shown below each plot. The hashed area indicates the systematic uncertainties on the model expectations.

eling of A^l_{FB} in W+jets production is required for the measurement of A^l_{FB} in $t\bar{t}$ events. The asymmetry has been measured precisely for inclusive W-boson production [37]. However, there are notable differences between inclusive W-boson production and the production of a W boson in association with jets, which constitutes the main background in this analysis. In particular, inclusive W-boson production is dominated by collisions between valence u and $\bar{d}$ (or d and $\bar{u}$) quarks. As the average momentum carried by u quarks is higher than that carried by d quarks, the W^+ bosons are preferentially boosted in the direction of the incoming proton. The boost of the W bosons leads to positive A^l_{FB} in inclusive W-boson production, which dominates over the negative contribution to A^l_{FB} due to the $V-A$ nature of W-boson decay. But in the W+jets events that pass the selection criteria of this analysis and contribute to the background, the rate and properties of the events that originate from interactions between valence quarks are different. In these events, the production of multiple jets reduces the boost of the W bosons relative to their boost in inclusive W production, leading to negative A^l_{FB}. Only 20%–40% of the W+jets background originates from interactions between valence quarks and the rest originates from quark–gluon interactions. In quark–gluon interactions, the W boson is produced from a valence quark, which is twice as likely to be a u rather than a d quark, and a soft antiquark from a gluon (or the charge conjugate process), leading to a large boost of the W boson and to positive A^l_{FB}.

We compare the simulated A^l_{FB} to the control data sample with three jets and zero b tags, which is dominated by W+jets background and is not used for measuring A^l_{FB} in $t\bar{t}$ events. The composition of the three-jet, zero-b-tag control sample cannot be determined reliably by applying the technique of the previous section solely within the control sample itself (see Fig. 4). Using the normalizations of the $t\bar{t}$ signal and multijet background from the fit of Section VII B, we predict their contributions in the control sample. We find that the control sample is dominated by W+jets background, with about 75% of events from W+jets production, 12% from multijet production, 9% from other backgrounds and 4% from $t\bar{t}$ production.

The differential asymmetry $A^l_{\text{FB}}(|y_l|)$ is constrained by continuity to be zero at $|y_l|=0$, hence at first order it is proportional to $|y_l|$. Figure 6 shows $A_{\text{CR}}(|y_l|)$, where A_{CR} is the A^l_{FB} of the W+jets background in the control region, and fits of $A_{\text{CR}}(|y_l|)$ to a line that passes through the origin for the W+jets simulation and for data. The control data is shown after subtraction of the estimated contributions from $t\bar{t}$, multijet, and other-background production.

We weight each event of the simulated W+jets background, regardless of its jet and b-tag multiplicities, using the function

$$w = 1 + \alpha q_l y_l, \qquad (3)$$

choosing α so that the simulated slope of $A_{\text{CR}}(|y_l|)$

(shown in Fig. 6 for $\alpha = 0$) agrees with the observed slope. Thus, we rely on the MC generators to describe the dependence of the W+jets A^l_{FB} on the number of jets and the number of b tags, and the resulting channel-to-channel differences in this asymmetry. The statistical uncertainty on α is taken from the statistical uncertainties on the slopes of the fits to both data and MC. The resulting differences ΔA_{CR} between the A_{CR} before and after the reweighting are larger than expected from the PDF uncertainties on A_{CR} (see Table IV). This raises the possibility that this tension is not entirely due to the choice of PDFs and leads us to assign the entire effect of the reweighting as a systematic uncertainty.

TABLE IV: Parameters of the $q_l y_l$ reweighting of the W+jets background, effects on A_{CR}, and PDF uncertainties. The first row lists the parameter α of the $q_l y_l$ reweighting with its statistical uncertainty. The second row lists the effect of the reweighting on A_{CR}. The next two rows list the up and down uncertainties on A_{CR} due to PDFs.

Quantity	p^l_T range, GeV			
	≥ 20	20–35	35–60	≥ 60
α, %	4.5 ± 1.8	7.9 ± 2.7	5.7 ± 2.4	-6.6 ± 4.3
ΔA_{CR}, %	2.7 ± 1.0	4.7 ± 1.6	3.3 ± 1.4	-3.9 ± 2.6
σ^+_{CR}, %	1.0	0.5	1.2	0.8
σ^-_{CR}, %	1.7	1.6	1.7	1.8

The $q_l y_l$ reweighting, using the control data, reduces the PDF uncertainties by at least a factor of three in each p^l_T range. However, for each p^l_T bin the uncertainties on the A^l_{FB} of the W+jets background from the reweighting procedure are more than twice the size of the simulated PDF uncertainties evaluated without the reweighting procedure.

The production-level measurement is affected by this $q_l y_l$ reweighting through the $q_l y_l$ distribution of the subtracted W+jets background. The reconstruction-level measurement is affected by this reweighting through ΔA_{CR}. The effect of the reweighting on the W+jets A^l_{FB} in each signal channel is within 0.3% of ΔA_{CR}.

VIII. UNFOLDING THE ASYMMETRIES

The inclusive A^l_{FB} is unfolded separately in each channel, and the measured A^l_{FB} values are then combined to form the inclusive measurement. Due to the excellent angular resolution for leptons, migrations in rapidity are negligible, and unfolding the A^l_{FB} reduces to correcting for acceptance effects. The inverse of the simulated selection efficiency is taken as a weight for each bin in $q_l y_l$ to correct for acceptance effects. These corrections therefore assume the SM as modeled in MC@NLO. We restrict the selection to $|y_l| < 1.5$ to avoid the region of low acceptance, and compute the weights in 48 bins as in the previous A^l_{FB} measurement [3].

For the differential A^l_{FB} measurement, we define for
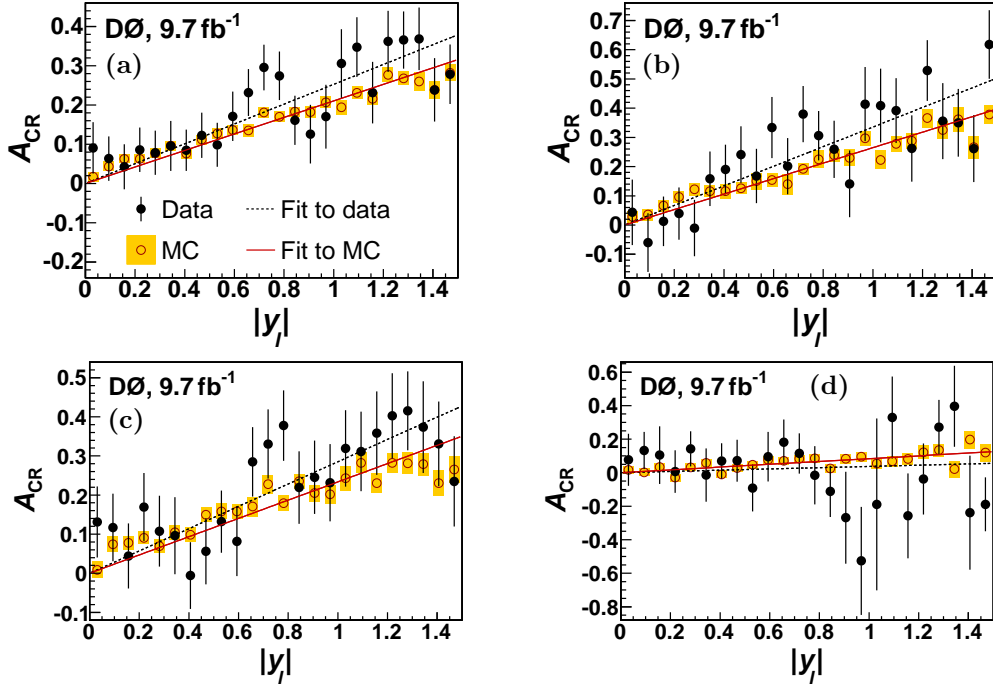
FIG. 6: The asymmetry of leptons from W+jets production as a function of $|y_l|$ for (a) the inclusive sample, (b) $20 \leq p_T^l < 35\,\mathrm{GeV}$, (c) $35 \leq p_T^l < 60\,\mathrm{GeV}$, and (d) $p_T^l \geq 60\,\mathrm{GeV}$. The points show the data from the control region, after the subtraction of the non-W+jets contributions, and the dashed line shows a fit to the functional form $y = ax$. The empty circles and solid line show the nominal W+jets simulation and its fit to the same functional form. The error bars and shaded regions indicate the statistical uncertainties on the data and simulation.

each of the 48 $q_l y_l$ bins a vector $\vec{r}$ of observed counts in the three p_T^l bins. The observed counts are affected by the migration of $\approx 10\%$ of the events over the bin boundaries in p_T^l. The expectation value of $\vec{r}$ is $\langle \vec{r} \rangle = \boldsymbol{A}\boldsymbol{M}\vec{p}$, where $\boldsymbol{A}$ is the acceptance matrix, $\boldsymbol{M}$ is the 3×3 migration matrix and $\vec{p}$ is the vector of production-level event counts. The acceptance matrix is a 3×3 diagonal matrix with the three acceptance probabilities embedded in its diagonal. The vector of the unfolded production-level counts that best estimates the vector $\vec{p}$ is $\vec{u} = \boldsymbol{A}^{-1}\boldsymbol{M}^{-1}\vec{r}$. With a nearly diagonal migration matrix and only three bins, the above matrix inversion yields stable solutions.

We evaluate the statistical uncertainty of the unfolded A_{FB}^l from each channel using an ensemble of pseudo-datasets that match the sample composition in data, with the signal simulated according to MC@NLO. The pseudo-datasets are simulated using Poisson fluctuations both on the selected sample and on the multijet control sample. The statistical uncertainties on A_{FB}^l for each channel and the weight of each channel in the combined measurement are listed in Table V.

Since the l+3 jet, zero-b-tag channel is used to tune the modeling of the W+jets background, it cannot be used to extract the signal A_{FB}^l. We also do not use the l+$\geq$4 jet, zero-b-tag channel for the unfolded result, due to its low purity and yield and due to the resulting large statistical and systematic uncertainties on A_{FB}^l expected in this

TABLE V: Statistical uncertainty (σ) on the measured A_{FB}^l and weight for each channel (where applicable). The weight for each channel is proportional to σ^{-2}.

Channel	σ	Weight
l+3 jets, 0 b tags	24%	n/a
l+3 jets, 1 b tag	6.8%	0.11
l+3 jets, $\geq$2 b tags	4.7%	0.24
l+$\geq$4 jets, 0 b tags	13.9%	n/a
l+$\geq$4 jets, 1 b tag	4.7%	0.24
l+$\geq$4 jets, $\geq$2 b tags	3.6%	0.41

channel. The weighted average of the four remaining b-tagged channels gives our combined value for A_{FB}^l.

The lepton-based asymmetries unfolded to the production level are summarized in Table VI and shown in Fig. 7. The results are compared to MC@NLO-based predictions.

We also measure the differential asymmetry as a function of $|y_l|$ by applying the same procedure that is used for the inclusive asymmetry to the $q_l y_l$ bins contained in each $|y_l|$ range. The measured differential asymmetries are listed in Table VII and shown in Fig. 8.

TABLE VI: Predicted and observed production-level asymmetries. The first uncertainty on the measured A_{FB}^l is statistical and the second systematic. The statistical uncertainties on the MC predictions are less than 0.1%, while the scale and PDF uncertainties are estimated to be < 1%.

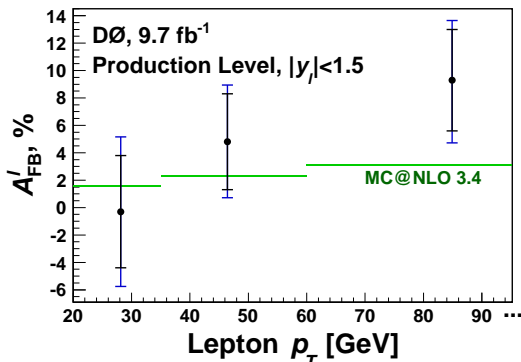| p_T^l range, GeV	A_{FB}^l, %	
	Data	MC@NLO
Inclusive	$4.2 \pm 2.3^{+1.7}_{-2.0}$	2.0
20–35	$-0.3 \pm 4.1 \pm 3.6$	1.6
35–60	$4.8 \pm 3.5^{+2.2}_{-2.1}$	2.3
≥ 60	$9.3 \pm 3.7^{+2.3}_{-2.7}$	3.1

FIG. 7: Predicted and observed production-level asymmetries as a function of lepton transverse momentum. The last bin extends beyond the edge of the plot and has no upper boundary. Statistical uncertainties are indicated by the inner, and the total uncertainties by the outer error bars.

TABLE VII: Predicted and observed production-level asymmetries as a function of $|y_l|$. The first uncertainty on the measured values is statistical and the second is systematic. The statistical uncertainties on the MC predictions are less than 0.1%, while the scale and PDF uncertainties are estimated to be < 1%.

$|y_l|$ range	A_{FB}^l, %	
	Data	MC@NLO
$0 - 0.125$	$0.5 \pm 6.1^{+0.8}_{-0.7}$	0.2
$0.125 - 0.375$	$0.5 \pm 4.4^{+1.3}_{-1.8}$	0.9
$0.375 - 0.625$	$2.6 \pm 4.7^{+1.7}_{-1.5}$	1.8
$0.625 - 1$	$1.9 \pm 4.6^{+2.0}_{-2.3}$	2.7
$1 - 1.5$	$13.2 \pm 6.5^{+2.6}_{-3.0}$	3.7

IX. SYSTEMATIC UNCERTAINTIES

We consider several sources of systematic uncertainty. For most sources, we vary the modeling according to the evaluated uncertainty in the relevant parameters of the model, repeat the entire analysis and propagate the effect to the final result. This accounts for the correlations between the channels and between the various steps of the analysis, such as the maximal likelihood fit, the
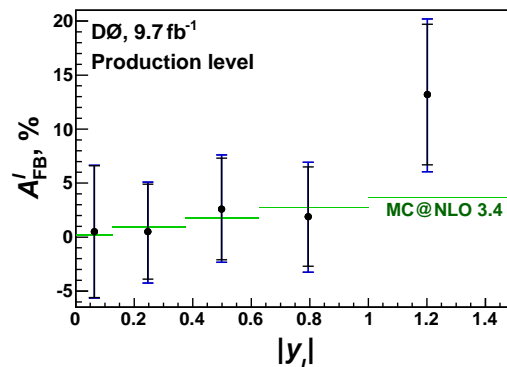

FIG. 8: Predicted and observed production-level asymmetries as a function of absolute lepton rapidity. Statistical uncertainties are indicated by the inner, and the total uncertainties by the outer error bars.

fit for α, and the unfolding. Some sources are quantified using more specialized procedures, as described below. Systematic uncertainties from different sources are added in quadrature to yield the total systematic uncertainty. Table VIII lists the systematic uncertainties on the predicted reconstruction-level A_{FB}^l (as listed in Tables I and II), on the measured reconstruction-level A_{FB}^l, and on the measured production-level A_{FB}^l. The systematic sources are classified into the following categories:

Jet reconstruction (reco)

This source includes the jet reconstruction and identification efficiencies, as well as the efficiency of the vertex confirmation described in Section V. The simulated efficiencies are calibrated on dijet data. Additional $p\bar{p}$ collisions within the same bunch crossing can yield additional jets, and their modeling is also included in this category. The rate of additional $p\bar{p}$ collisions is derived from the number of reconstructed vertices per event.

Jet energy measurement

The jet energy scale (JES) is measured using dijet and photon+jet samples [38]. The simulated jet energy resolution (JER) is calibrated using Z+jet data. Their uncertainties are propagated to the measured asymmetry.

Signal modeling

As discussed in Section VI, the SM predicts a negative asymmetry for events with additional final state gluons (and hence with larger $p_T^{t\bar{t}}$). Thus, event selection introduces a bias on the measured asymmetry, in particular making it sensitive to the jet multiplicity. The inclusion of $l+3$ jet events in the analysis reduces this correlation. To evaluate the size of this systematic effect we vary the amount of initial-state radiation (ISR) within an uncertainty range established from a measurement of ISR rates [39].

Forward-backward differences in the amount of ad-

ditional radiation can also affect the measurement through $p_T^{t\bar{t}}$, which is correlated with the acceptance [3]. These differences are controlled by the simulated color coherence of the partonic showers [3]. QCD predicts that parton showers in angular order are more likely, while the simulation enforces strict angular ordering [36]. NLO event generators calculate the first QCD emission analytically, reducing the reliance on the modeling of the parton showers. To quantify this uncertainty, we consider the possibility that the dependence of $A_{\rm FB}^l$ on $p_T^{t\bar{t}}$ is 25% smaller than in MC@NLO, a possibility motivated by the studies of Ref. [36].

The $p_T^{t\bar{t}}$ distribution was studied in Refs. [5, 40] and found to be well modeled. This is in contrast to the limitations of the D0-detector simulation, which result in poor modeling of this distribution [3]. We consider the possibility that this mismodeling also affects $A_{\rm FB}^l$ by reweighting the simulated events as a function of the reconstructed $p_T^{t\bar{t}}$ so that the $p_T^{t\bar{t}}$ distribution agrees with data.

The mass of the top quark was varied from its value in the nominal simulation of 172.5 GeV according to the latest measurement [8]. To quantify additional systematic uncertainties due to the modeling of signal, we repeat the analysis using signal events simulated with ALPGEN combined with PYTHIA. As the box diagram is not included in ALPGEN, ALPGEN predictions are missing the largest contribution to the $t\bar{t}$ asymmetry [1]. Furthermore, this missing contribution peaks at low $p_T^{t\bar{t}}$, where acceptance is low, making the acceptance predicted by ALPGEN unrealistic. Therefore we use the acceptance predicted by MC@NLO instead of the one predicted by ALPGEN in evaluating this uncertainty.

The uncertainties on the production-level inclusive $A_{\rm FB}^l$ due to the top quark mass, the choice of MC generator, and the overall amount of ISR are similar. The systematic uncertainties due to the forward-backward differences in the additional radiation and due to $p_T^{t\bar{t}}$ reconstruction have negligible effect on the inclusive $A_{\rm FB}^l$.

b tagging

The b-tagging efficiency and mistagging probability, which are determined from dijet data with at least one muon identified within a jet, affect the division of events between 0, 1, and ≥ 2 b-tag subsamples. Due to this division of channels, the analysis is now more sensitive to systematic variations on b-tagging than the previous measurement [3].

Background (Bg) subtraction

The subtracted amounts of W+jets and multijet background are varied within their fitted uncertainties. Uncertainties on the normalization and shape of the multijet background arise from the uncertainties on the lepton selection rates, which

are used to evaluate the multijet background. An uncertainty of 20% is assigned to the rate of $W + c\bar{c}$ and $W + b\bar{b}$ production.

Background (Bg) modeling

The $q_l y_l$ reweighting of the W+jets background is varied using α values of zero and twice the nominal α (see Table IV). The effect of increased multijet production at large $|y_l|$ is considered by reweighting the multijet $q_l y_l$ distribution to better match the data in the $l+3$ jet, zero-b-tag control region. The possibly underestimated muon background with mismeasured high transverse momentum described in Section V peaks in that region, and an excess of data events in that region is seen in some channels. We also consider a similar increase in W+jets production at large $|y_l|$.

We account for the marginal agreement of the dijet invariant mass (see Fig. 3c) and related observables between data enriched in W+jets production and the ALPGEN simulation of such data [41] by reweighting the simulated $M_{jj}^{\min}$ distribution of the W+jets background to match data in the $l+3$ jet, 0-b-tag control region. This improves the modeling of $M_{jj}^{\min}$ in all channels, supporting the attribution of this small mismodeling to the modeling of W+jets production. A small mismodeling of $\Delta\phi({\rm jet}_1, \not{E}_T)$ is indicated in Fig. 3e, but its effect on the discriminant is far smaller than that of the region around $M_{jj}^{\min} = 50$ GeV.

Parton distribution functions

Each of the error eigenvectors of the set of PDFs is varied up and down, and the effects are added in quadrature. We also consider an uncertainty due to the choice of PDFs, which we evaluate using the nominal PDFs of the CTEQ6L1 [42] and MRST2003 [43] sets. The MRST2003 set is chosen since its u, d, s, and g PDFs differ significantly from those of the CTEQ6L1 set for values of Bjorken x above 0.01, which are the most relevant to this analysis.

TABLE VIII: Systematic uncertainties on $A_{\rm FB}^l$. Uncertainties smaller than 0.1% are omitted.

| | Absolute uncertainty, % | | |
| | Reconstruction level | | Prod. level |
Source	Prediction	Measurement	Measurement
Jet reco	−0.1	–	–
JES/JER	+0.1	+0.1/−0.3	+0.2/−0.3
Signal modeling	–	−0.2	+0.6/−0.4
b tagging	±0.1	+0.5/−0.8	+0.8/−1.1
Bg subtraction	n/a	+0.1/−0.3	+0.1/−0.3
Bg modeling	n/a	+1.4/−1.5	+1.3/−1.5
PDFs	–	+0.3/−0.2	+0.1/−0.2
Total	±0.1	+1.5/−1.7	+1.7/−2.0

X. DISCUSSION

Using a dataset corresponding to an integrated luminosity of $9.7\,\mathrm{fb}^{-1}$, we measure the production-level inclusive A_{FB}^l to be $\left(4.2 \pm 2.3\,(\mathrm{stat.})^{+1.7}_{-2.0}\,(\mathrm{syst.})\right)\%$. The previously published value, which was measured using a subset of this dataset corresponding to $5.4\,\mathrm{fb}^{-1}$ [3], is $A_{\mathrm{FB}}^l = (15.2 \pm 4.0)\%$. In this section we further compare these measurements and discuss the reasons for the difference between their results. Unlike the previous measurement, the current result is in good agreement with the MC@NLO prediction for the production-level of $A_{\mathrm{FB}}^l = 2.0\%$, which has a statistical uncertainty of less than 0.1%. The statistical uncertainty on the measured A_{FB}^l is reduced by a factor of ≈ 1.67 with respect to Ref. [3]. This reduction is mostly due to the addition of new data (by 1.30) and the inclusion of events with three jets (by 1.25).

The inclusion of $l+3$ jet events, the addition of newer data, the use of better object identification algorithms, and improvements to the analysis technique all decrease the measured asymmetry. Both here and in Ref. [3], the analysis strategy and all details that would affect the measured central value were finalized on the basis of Monte Carlo and control data before analyzing the selected data events. Together, these changes reduce the measured A_{FB}^l by 10.5%, yet no single change accounts for a difference of more than 3%. These changes are detailed in Table IX for the reconstruction-level asymmetry, which should be compared to the predictions listed in this table. The largest change in the measured A_{FB}^l occurs when switching from the b tagging algorithm used in Ref. [3] (described in Ref. [44]) to the one used in this analysis [26]. In both cases, the b-tagging algorithm was chosen and optimized based on studies of dijet data, and the choice of algorithm was not specific to the analysis. Table IX also shows that the changes due to the asymmetry of the backgrounds are fairly small. We note that the effect of the W+jets reweighting on the inclusive A_{FB}^l in the full sample (1.4%) is smaller than in the sample corresponding to the first $5.4\,\mathrm{fb}^{-1}$ (2.1% as listed in Table IX).

The p-value for the previously published value, assuming the asymmetry predicted by MC@NLO, is 1.7×10^{-3}, while the p-value of the new result is 0.24. These numbers do not account for the systematic uncertainty on the theoretical predictions.

Most of the asymmetry in the previous analysis is contained in the $l+\geq 4$ jets channel for events with exactly one b tag. In the current analysis, the asymmetry in this channel is still high compared to the SM expectation, with $A_{\mathrm{FB}}^l = \left(16.3 \pm 4.8\,(\mathrm{stat.})^{+2.2}_{-1.4}\,(\mathrm{syst.})\right)\%$. The relative weight of this channel decreased from $\approx 50\%$ in the previous analysis to 24% in the current analysis. The $q_l y_l$ distributions in each channel are shown in Fig. 5. The A_{FB}^l values of the various channels are compared in Fig. 9, Table X and Table XI. The consistency between different channels in Fig. 9 corresponds to a χ^2 value of

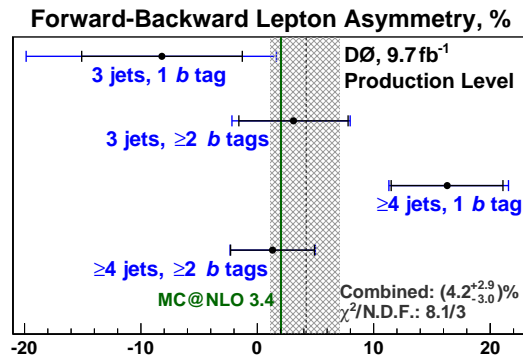8.1 for three degrees of freedom, which corresponds to a tail probability of 4.5%.

FIG. 9: Measured production-level A_{FB}^l by analysis channel. The vertical line shows the MC@NLO prediction. The χ^2 is of a fit to a single value, shown by the crosshatched band and the dashed line. Statistical uncertainties are indicated by the inner vertical lines, and the total uncertainties by the vertical end lines.

We also studied the asymmetry in subsamples defined by the charge of the lepton, the flavor of the lepton, and by the polarities of the D0 magnets, which are reversed every two weeks. Reversing the magnet polarities greatly reduces possible experimental biases which involve the lepton. All measurements agree within at most two standard deviations. For example, in the e+jets channels we find a reconstruction-level asymmetry of $A_{\mathrm{FB}}^l = (3.4 \pm 2.8\,(\mathrm{stat.}))\%$ and in the μ+jets channels we find a reconstruction-level asymmetry of $A_{\mathrm{FB}}^l = (1.6 \pm 3.1\,(\mathrm{stat.}))\%$, which are to be compared to the simulated values of $A_{\mathrm{FB}}^l = (1.3 \pm 0.1\,(\mathrm{stat.}))\%$ and $A_{\mathrm{FB}}^l = (2.1 \pm 0.2\,(\mathrm{stat.}))\%$, respectively.

Since the SM-derived corrections to the measured A_{FB}^l are only 1–2%, the dependence of the results on the SM is small and the results may be validly compared to the predictions of beyond the SM predictions. We tested our analysis method using axigluon samples produced using MADGRAPH combined with PYTHIA with axigluon masses of 0.2, 0.4, 0.8, and $2\,\mathrm{TeV}$ with completely left-handed, completely right-handed and mixed couplings [45]. In all of these scenarios, the measured production-level A_{FB}^l exhibits additional, model-dependent scatter about the simulated A_{FB}^l values of $< 1.5\%$ (absolute).

XI. COMBINATION AND EXTRAPOLATION

The D0 Collaboration measured A_{FB}^l in the dilepton channel, with lepton coverage that extends to $|y_l| = 2$, finding $A_{\mathrm{FB}}^l = \left(4.1 \pm 3.5\,(\mathrm{stat.}) \pm 1.0\,(\mathrm{syst.})\right)\%$ [4]. To enable a direct combination with the measurements in the l+jets channel, the analysis of Ref. [4] is repeated using only leptons with $|y_l| < 1.5$, finding $A_{\mathrm{FB}}^l = \left(4.3 \pm 3.4\,(\mathrm{stat.}) \pm 1.0\,(\mathrm{syst.})\right)\%$. The decrease in the statistical uncertainty is due to the removal of the events with $|y_l| >$

TABLE IX: Reconstruction-level A_{FB}^l from Ref. [3] to this analysis, with six intermediate steps. The first column indicates what changed from the previous step. The second and third columns list the simulated and measured $t\bar{t}$ asymmetries. The fourth column lists the "raw" asymmetry of the selected events, before background subtraction. The last two columns list the asymmetries of the main components of the background model.

| | | | A_{FB}^l, % | | |
Step	$t\bar{t}$, predicted	$t\bar{t}$, measured	Raw	Multijet	W+jets
As in Ref. [3]	0.8 ± 0.6	14.2 ± 3.8	–	–	–
Obj. ID, data quality	0.7 ± 0.2	12.1 ± 3.6	11.4 ± 2.4	6.1 ± 4.3	13.1 ± 1.2
b tagging	0.7 ± 0.2	9.7 ± 3.5	9.8 ± 2.5	8.2 ± 4.8	10.7 ± 1.7
Rest of selection	0.8 ± 0.2	9.0 ± 3.5	9.3 ± 2.5	7.9 ± 4.5	12.7 ± 1.1
Multiple channels	0.8 ± 0.2	8.1 ± 3.5	9.3 ± 2.5	7.9 ± 4.5	12.7 ± 1.1
Added new channels	1.5 ± 0.1	6.0 ± 2.7	8.5 ± 1.3	8.3 ± 2.0	11.8 ± 0.5
W+jets reweighting	1.5 ± 0.1	3.9 ± 2.7	8.5 ± 1.3	8.3 ± 2.0	15.8 ± 0.5
Including newer data	1.6 ± 0.1	2.9 ± 2.1	7.7 ± 1.0	5.6 ± 1.4	15.0 ± 0.4

TABLE X: Measured and predicted A_{FB}^l by channel, at reconstruction level.

| | A_{FB}^l, % | |
Channel	Data	MC@NLO
l+3 jets, 1 b tag	$-6.8 \pm 6.0\,(\mathrm{stat.})^{+6.1}_{-5.6}\,(\mathrm{syst.})$	2.7 ± 0.4
l+3 jets, ≥ 2 b tags	$3.7 \pm 4.3\,(\mathrm{stat.})^{+1.1}_{-1.2}\,(\mathrm{syst.})$	2.8 ± 0.3
l+≥ 4 jets, 1 b tag	$14.8 \pm 4.2\,(\mathrm{stat.})^{+1.1}_{-1.2}\,(\mathrm{syst.})$	0.5 ± 0.3
l+≥ 4 jets, ≥ 2 b tags	$-0.9 \pm 3.2\,(\mathrm{stat.})^{+0.3}_{-0.9}\,(\mathrm{syst.})$	1.1 ± 0.2
Total	$2.9 \pm 2.1\,(\mathrm{stat.})^{+1.5}_{-1.7}\,(\mathrm{syst.})$	1.6 ± 0.2

TABLE XI: Measured A_{FB}^l by channel at production level. The MC@NLO prediction for $|y_l| < 1.5$ is $A_{\mathrm{FB}}^l = 2.0\%$.

Channel	Measured A_{FB}^l, %
l+3 jets, 1 b tag	$-8.2 \pm 6.9\,(\mathrm{stat.})^{+7.0}_{-9.4}\,(\mathrm{syst.})$
l+3 jets, ≥ 2 b tags	$3.1 \pm 4.7\,(\mathrm{stat.})^{+1.3}_{-2.4}\,(\mathrm{syst.})$
l+≥ 4 jets, 1 b tag	$16.3 \pm 4.8\,(\mathrm{stat.})^{+2.2}_{-1.4}\,(\mathrm{syst.})$
l+≥ 4 jets, ≥ 2 b tags	$1.3 \pm 3.6\,(\mathrm{stat.})^{+0.8}_{-0.5}\,(\mathrm{syst.})$
Total	$4.2 \pm 2.3\,(\mathrm{stat.})^{+1.7}_{-2.0}\,(\mathrm{syst.})$

1.5, which have a large weight due to the acceptance corrections and thus increase the statistical uncertainty.

This result is combined with the results of the current measurement using the Best Linear Unbiased Estimator (BLUE) method, as described in Ref. [46]. Systematic uncertainties are classified by their source as either completely correlated, e.g., the b tagging uncertainties, or completely uncorrelated, e.g., the background modeling uncertainties. The combination is a weighted average of the input measurements, with the dilepton measurement given a weight of 0.43 and the l+jets measurement a weight of 0.57. The combined value of A_{FB}^l for $|y_l| < 1.5$ is $A_{\mathrm{FB}}^l = \left(4.2 \pm 2.0\,(\mathrm{stat.}) \pm 1.4\,(\mathrm{syst.})\right)\% = (4.2 \pm 2.4)\,\%$.

The measurements are extrapolated to cover the full phase space using the MC@NLO simulation. Extrapolation adds nothing to our experimental measurements

of A_{FB}^l, but simply extends them by incorporating SM-inspired predictions for $t\bar{t}$ production outside the lepton rapidity coverage, thus facilitating comparison with theoretical calculations and the combination of the measurements. Such extrapolated values should not be compared with non-SM predictions [47]. To include dilepton events with $1.5 < |y_l| < 2$ in the extrapolated values, we extrapolate each result independently before combining them. If we assume a linear dependence of the asymmetry on $|y_l|$, we find an extrapolated asymmetry which is proportional to the measured asymmetry,

$$A_{\mathrm{FB}}^{l,\mathrm{ex}} = A_{\mathrm{FB}}^l A_{\mathrm{FB}}^{l,\mathrm{tot}} / A_{\mathrm{FB}}^{l,\mathrm{pred}}, \qquad (4)$$

where $A_{\mathrm{FB}}^{l,\mathrm{tot}}$ is the simulated A_{FB}^l in the entire phase space and $A_{\mathrm{FB}}^{l,\mathrm{pred}}$ is the simulated A_{FB}^l within the acceptance. For the simulated $t\bar{t}$ samples, such an extrapolation overestimates the fully inclusive A_{FB}^l. Furthermore, only the leading order of the $t\bar{t}$ asymmetry has been calculated, and so the dependence of A_{FB}^l on $|y_l|$ is not known precisely. Therefore we assign a systematic uncertainty to the extrapolation that equals the entire effect of the extrapolation. Using the MC@NLO predictions of $A_{\mathrm{FB}}^{l,\mathrm{tot}} / A_{\mathrm{FB}}^{l,\mathrm{pred}} = 1.19$ for the l+jets measurement and 1.07 for the dilepton measurement, and find a combined extrapolated asymmetry of $A_{\mathrm{FB}}^{l,\mathrm{ex}} = \left(4.7 \pm 2.3\,(\mathrm{stat.}) \pm 1.5\,(\mathrm{syst.})\right)\%$.

XII. SUMMARY

Using the full dataset collected by the D0 experiment during Run II of the Tevatron, corresponding to $9.7\,\mathrm{fb}^{-1}$, we have measured the forward-backward asymmetry in the direction of leptons from $t\bar{t}$ events in the l+jets channel and compared it to a prediction based on MC@NLO. Since the lepton-based asymmetry does not require a full reconstruction of the $t\bar{t}$ event, this measurement also uses events with only three jets. The measured asymmetry at production level for $|y_l| < 1.5$ is $A_{\mathrm{FB}}^l = \left(4.2^{+2.9}_{-3.0}\right)\%$.

We combined this measurement with the measurement in the dilepton channel and found a production-level

asymmetry for $|y_l| < 1.5$ of $A_{\mathrm{FB}}^l = (4.2 \pm 2.4)\,\%$, to be compared to the MC@NLO prediction of 2.0%. We have presented the first measurement of the differential asymmetry as a function of p_T^l. All results are in agreement with MC@NLO predictions.

Acknowledgments

[1] J. H. Kühn and G. Rodrigo, Phys. Rev. Lett. **81**, 49 (1998).

[2] W. Bernreuther and Z. G. Si, Nucl. Phys. B **837**, 90 (2010); W. Hollik and D. Pagani, Phys. Rev. D **84**, 093003 (2011).

[3] V. M. Abazov *et al.* [D0 Collaboration], Phys. Rev. D **84**, 112005 (2011).

[4] V. M. Abazov *et al.* [D0 Collaboration], Phys. Rev. D **88**, 112002 (2013).

[5] T. Aaltonen *et al.* [CDF Collaboration], Phys. Rev. D **87**, 092002 (2013).

[6] W. Bernreuther and Z.-G. Si, Phys. Rev. D **86**, 034026 (2012); private communications with W. Bernreuther, updating the error estimates.

[7] N. Kidonakis, Phys. Rev. D **84**, 011504 (2011); V. Ahrens *et al.*, Phys. Rev. D **84**, 074004 (2011).

[8] T. Aaltonen *et al.* [CDF and D0 Collaborations], Phys. Rev. D **86**, 092003 (2012).

[9] E.g., J. A. Aguilar-Saavedra, Nuovo Cim. C **035N3**, 167 (2012).

[10] V. M. Abazov *et al.* [D0 Collaboration], Phys. Rev. Lett. **100**, 142002 (2008).

[11] M. T. Bowen, S. D. Ellis, and D. Rainwater, Phys. Rev. D **73**, 014008 (2006).

[12] V. M. Abazov *et al.* [D0 Collaboration], Phys. Rev. D **87**, 011103(R) (2013).

[13] T. Aaltonen *et al.* [CDF Collaboration], Phys. Rev. D **88**, 072003 (2013).

[14] S. Frixione and B. R. Webber, J. High Energy Phys. 06 (2002) 029; S. Frixione *et al.*, J. High Energy Phys. 08 (2003) 007.

[15] J. M. Campbell and R. K. Ellis, arXiv:1204.1513 [hep-ph] (2012).

[16] E.g., D. Choudhury, R. M. Godbole, S. D. Rindani, and P. Saha, Phys. Rev. D **84**, 014023 (2011); E.L. Berger, Q.-H. Cao, C.-R. Chen, and H. Zhang, Phys. Rev. D **88**, 014033 (2013).

[17] A. Falkowski, M. L. Mangano, A. Martin, G. Perez, and J. Winter, Phys. Rev. D **87**, 034039 (2013).

[18] V. M. Abazov *et al.* [D0 Collaboration], Nucl. Instrum. Meth. A **565**, 463 (2006); M. Abolins *et al.*, Nucl. Instrum. Meth. A **584**, 75 (2008); B. C. K. Casey *et al.*, Nucl. Instrum. Meth. A **698**, 208 (2012).

[19] S. N. Ahmed *et al.*, Nucl. Instrum. Meth. A **634**, 8 (2011).

[20] R. Angstadt *et al.*, Nucl. Instrum. Meth. A **622**, 298 (2010);

[21] S. Abachi *et al.*, Nucl. Instrum. Meth. A **338**, 185 (1994).

[22] V. M. Abazov *et al.*, Nucl. Instrum. Meth. A **552**, 372 (2005).

[23] V. M. Abazov *et al.* [D0 Collaboration], Phys. Rev. D **84**, 012008 (2011).

[24] V. M. Abazov *et al.* [D0 Collaboration], Phys. Rev. D **76**, 092007 (2007); V. M. Abazov *et al.* [D0 Collaboration], Nucl. Instrum. Meth. A **737**, 281 (2014); V. M. Abazov *et al.* [D0 Collaboration], Nucl. Instrum. Meth. A **750**, 78 (2014).

[25] V. M. Abazov *et al.* [D0 Collaboration], Phys. Rev. D **88**, 092001 (2013).

[26] V. M. Abazov *et al.* [D0 Collaboration], submitted to Nucl. Instrum. Meth. A, arXiv:1312.7623 [hep-ex]. In this analysis, jets with MVA > 0.035 are tagged.

[27] G. Corcella *et al.*, J. High Energy Phys. 01 (2001) 010.

[28] M. L. Mangano *et al.*, J. High Energy Phys. 07 (2003) 001.

[29] T. Sjöstrand *et al.*, Comput. Phys. Commun. **135**, 238 (2001).

[30] J. M. Campbell and R. K. Ellis, Nucl. Phys. Proc. Suppl. **205**, 10 (2010).

[31] V. M. Abazov *et al.* [D0 Collaboration], Phys. Lett. B **693**, 522 (2010).

[32] C. Balazs and C. P. Yuan, Phys. Rev. D **56**, 5558 (1997).

[33] E. Boos *et al.* [CompHEP Collaboration], Nucl. Instrum. Meth. A **534**, 250 (2004).

[34] V. M. Abazov *et al.* [D0 Collaboration], Phys. Rev. D **83**, 032009 (2011).

[35] S. S. Snyder, Doctoral Thesis, State University of New York at Stony Brook (1995), FERMILAB-THESIS-1995-27.

[36] P. Skands, B. Webber, and J. Winter, J. High Energy Phys. 07 (2012) 151.

[37] V. M. Abazov *et al.* [D0 Collaboration], Phys. Rev. D **88**, 091102 (2013); T. Aaltonen *et al.* [CDF Collaboration], Phys. Rev. Lett. **102**, 181801 (2009).

[38] V. M. Abazov *et al.* [D0 Collaboration], accepted to Nucl. Instrum. Meth. A, arXiv:1312.6873 [hep-ex].

[39] V. M. Abazov *et al.* [D0 Collaboration], Phys. Rev. Lett. **106**, 122001 (2011).

[40] G. Aad *et al.* [ATLAS Collaboration], Eur. Phys. J. C **73**, 2261 (2013); S. Chatrchyan *et al.* [CMS Collaboration], Eur. Phys. J. C **73**, 2339 (2013).

[41] E.g., the Jet ΔR reweighting of T. Aaltonen *et al.* [CDF Collaboration], Phys. Rev. D **82**, 112005 (2010).

[42] J. Pumplin *et al.*, J. High Energy Phys. 07 (2002) 012;

D. Stump *et al.*, J. High Energy Phys. 10 (2003) 046.

[43] A. D. Martin, R. G. Roberts, W. J. Stirling, and R. S. Thorne, Eur. Phys. J. C **35**, 325 (2004).

[44] V. M. Abazov *et al.* [D0 Collaboration], Nucl. Instrum. Meth. A **620**, 490 (2010). In Ref. [3], jets with NN output of more than 0.2 are tagged.

[45] J. Alwall, M. Herquet, F. Maltoni, O. Mattelaer, and T. Stelzer, J. High Energy Phys. 06 (2011) 128.

[46] L. Lyons, D. Gibaut, and P. Clifford, Nucl. Instrum. Methods Phys. Res. A **270**, 110 (1988); A. Valassi, Nucl. Instrum. Methods Phys. Res. A **500**, 391 (2003).

[47] M. I. Gresham, I. -W. Kim and K. M. Zurek, Phys. Rev. D **83**, 114027 (2011).